Advanced Healthcare Materials

ADVANCED HEALTHCARE MATERIALS
www.advhealthmat.de

RESEARCH ARTICLE

3D Printed Silk Fibroin-Gelatin Construct Targeting BMP Signaling for Articular Cartilage Regeneration Within a Full-Thickness Cartilage Defect in a Surgically Induced Osteoarthritic Rat Knee Joint

Sayeda Fauzia Iqbal[1,2] | Nilotpal Majumder[3] | Bhupendra Kumar[1,2] | Chandrashish Roy[3] | Saahiba Thaleshwari[1,2] | Sourabh Ghosh[3] | Amitabha Bandyopadhyay[1,2]

[1]Department of Biological Sciences and Bioengineering, Indian Institute of Technology Kanpur, Kanpur, Uttar Pradesh, India | [2]The Mehta Family Centre for Engineering in Medicine, Indian Institute of Technology Kanpur, Kanpur, Uttar Pradesh, India | [3]Department of Textile and Fibre Engineering, Indian Institute of Technology Delhi, New Delhi, Delhi, India

Correspondence: Sourabh Ghosh (sourabh.ghosh@textile.iitd.ac.in) | Amitabha Bandyopadhyay (abandopa@iitk.ac.in)

Received: 23 December 2025 | **Revised:** 27 April 2026 | **Accepted:** 2 May 2026

Keywords: articular cartilage | BMP | cartilage regeneration | osteoarthritis | silk-fibroin

ABSTRACT

Regenerating articular cartilage within osteoarthritis (OA)-affected joints remains a long-standing challenge. This study introduces a novel chemically modified silk-based biomaterial to modulate key signaling pathways involved in OA and cartilage repair. The designed biomaterial concurrently inhibits the bone morphogenetic protein (BMP) signaling, aberrantly activated during OA, and inherently facilitates Wnt/β-catenin signaling, a crucial factor for chondrogenesis and cartilage homeostasis. The dual modulation was achieved by covalently conjugating the potent BMP inhibitor LDN-193189 to the Silk Fibroin–Gelatin (SF-G) bioink. The chemically decorated SF-G construct served as a biomimetic delivery platform and a mechanically robust support, ideally suited for regenerating load-bearing articular cartilage. The functionalized material was implanted into a critical-sized cartilage defect in the rat femoral trochlear groove, which had been previously subjected to OA by anterior cruciate ligament transection. The results confirmed successful neocartilage regeneration, evidenced by dense Safranin O staining and expression of cartilage-specific collagen. The absence of hypertrophic markers, fibrocartilage, and inflammation indicates the authenticity of hyaline cartilage formation in a severe OA microenvironment. Overall, the LDN-193189-conjugated SF-G construct overcame the challenges of maintaining phenotypic stability in articular cartilage of OA joints, representing a promising regenerative approach for restoring lost cartilage.

1 | Introduction

Osteoarthritis (OA) affects more than 500 million people worldwide, with its predicted burden increasing dramatically in the coming decade [1]. Considered a disease of the knee joint, articular cartilage degeneration is a hallmark of OA progression, with its etiology ranging from age, excessive physical exertion, mechanical injury, or metabolic disorders such as obesity or hyperglycemia [2, 3]. Existing treatment modalities are limited to disease-modifying pharmacological agents aimed at pain

Sayeda Fauzia Iqbal and Nilotpal Majumder contributed equally to this work.

management or surgical procedures (Unicompartmental or Total Knee Arthroplasty (TKA)) in extreme clinical scenarios [4, 5]. Apart from being expensive, TKA is often associated with serious deterioration of quality of life, with increased chances of infections and joint morbidity at the surgery site [4]. Therefore, the primary aim of treatment modalities should be to achieve permanent solutions, such as regenerating the degenerated articular cartilage at the inflamed joint site.

Articular cartilage is the most affected tissue type in OA, marked by extensive degradation of extracellular matrix (ECM) components, apoptosis of tissue-resident chondrocytes, matrix calcification, and neovascularization [6]. Several attempts have been made in recent decades to engineer articular cartilage in vitro using a range of biomaterials [7, 8], cell sources [9, 10], fabrication methods [11, 12], and culture conditions [13]. Although engineered articular cartilage grafts demonstrate anatomical and molecular traits similar to those of native cartilage, none of these strategies have yet rendered clinically feasible outcomes that completely abrogate OA progression and simultaneously promote neo-cartilage regeneration. A major reason for this blockade lies in the poor understanding of the molecular signatures associated with the physiological alterations of articular cartilage and its surrounding microenvironment during the pathological progression of OA. Our understanding is limited to the degenerative nature of articular cartilage, characterized by a highly degraded ECM, hypertrophic chondrocytes (enlarged and aggregated), and loss of matrix elasticity, which inhibits natural healing and can lead to ossification of the remaining cartilage tissue [14, 15]. Additionally, the roles of reactive oxygen species (ROS) [16], chronic inflammation, and increased proteases [17] in the surrounding niche exacerbate chondrocyte apoptosis and matrix degradation, as well documented. However, the reasons for these failed strategies remain unaddressed, as the rationale for these unwarranted physiological occurrences remains unclear.

A key cellular event for such an aberrant physiological phenomenon in the articular cartilage tissue is the "chondrocyte hypertrophy and hypersecretion", molecularly defined by the activation of several pro-osteogenic signaling pathways like Indian Hedgehog (IHH) [18, 19], Bone morphogenetic protein (BMP) [20], etc., further leading to a "bone-like" vascularized tissue formation with enhanced expression levels of osteogenic markers like matrix metalloproteases (MMP1/13), runt related transcription factor (RUNX2), collagen type X alpha chain (COL10A1) [21]. A plethora of reasons has been hypothesized for the occurrence of hypertrophy during in vitro chondrogenesis, including regular chondrogenic media supplements [21], a hypoxic microenvironment [22], or imbalanced mechanical loading [23], which contribute to the onset of hypertrophic differentiation of stem cells or chondrocytes. However, in the adult knee joint, hypertrophic differentiation of chondrocytes is triggered by the requirement of stiffer cartilage matrix, i.e., collagen type X (ColX), to compensate for the uneven mechanical loading due to injury or loss of cartilage integrity. BMP signaling is a major regulator of hypertrophic differentiation. BMP2/4 is significantly upregulated in human osteoarthritic tissues [24]. Pre-treating engineered cartilage with a BMP inhibitor helps to maintain its hyaline characteristics when implanted subdermally in an ex vivo model [25]. Recently, Jaswal et al. also demonstrated that in situ inhibition of BMP signaling blocks the progression of OA, even when administered after the onset of surgically induced OA in a mouse model [20]. Suppressing osteoarthritic influence is a formidable challenge during the implantation of tissue-engineered cartilage grafts; biomaterial-assisted neocartilage regeneration is underway. Current strategies, such as microfracture and autologous chondrocyte implantation, can result in hypertrophy and the formation of fibrocartilage. Sustained delivery of BMP signaling inhibitor in the intra-articular cavity can provide an anti-catabolic environment by further repressing chondrocyte hypertrophy and inflammatory conditions, and promote deposition of cartilage ECM.

Silk fibroin is an FDA-approved, versatile biomaterial widely used by researchers worldwide for various biomedical applications [26]. The unique, tailorable mechanics, biocompatibility, and ease of chemical modifications have rendered it useful for engineering a range of hard and soft tissues, including meniscus [27], load-bearing bones [28], nerve conduits [29], and skin [30]. Prior research from our lab has demonstrated the advantages of using SF-G bioink and 3D bioprinting technology to fabricate tissue-engineered cartilage constructs, elucidating various aspects of cartilage tissue engineering. A comparison study of 3D spheroids and dispersed human bone marrow-derived mesenchymal stem cells (hBMSCs) and articular chondrocytes, embedded within SF-G bioink, demonstrated that chondrocytes exhibit superior anti-hypertrophic characteristics over hBMSCs [31]. Chawla et al. have also demonstrated the pro-chondrogenic role of encapsulated murine BMSCs, in addition to the inherent upregulation of the Wnt/β-catenin pathway by the SF-G bioink, a key signaling cascade that regulates chondrogenesis and cartilage homeostasis [32–34]. However, exogenous supplementation of the biochemical mediators in the culture medium requires frequent replenishment due to their short half-lives, like 24 h for TGFβ3 or 4 h for LDN-193189, which reduces their bioavailability and makes the process expensive. This challenge was addressed by Majumder et al., who demonstrated the superiority of covalent conjugation over exogenous supplementation for the overall chondrogenic profile of hBMSCs [9]. They further investigated the potential of the chemically modified SF-G bioink for chondrogenic differentiation and for maintaining a stable chondrogenic phenotype under in vitro OA-mimicking conditions [35]. In this study, different pro-chondrogenic and anti-hypertrophic small molecules (LDN-193189, TGFβ3, and Interleukin 1 receptor antagonist (IL-1Ra)) were covalently conjugated to SF-G bioink to impart sustained delivery to hBMSCs [35]. Additionally, they demonstrated down-regulation of the Wnt pathway inhibitor Dickkopf (DKK) in the LDN-193189-conjugated SF-G 3D bioprinted group encapsulated with human BMSCs. This indicated upregulation of the Wnt/β-catenin pathway, which maintained a stable articular cartilage phenotype when primed under in vitro OA-mimicking conditions [35]. However, evaluating the anti-hypertrophic properties and neo-cartilage regeneration of the tissue-engineered product in an animal model is of utmost importance, given the more complex joint niche, which involves a multitude of cell types and inflammatory cytokine cocktails. Several reports have shown that engineered cartilage constructs can heal cartilage defects in vivo when transplanted into full-thickness defects [36–38]. Nevertheless, none of the studies reported regeneration of the full-thickness cartilage defect in an osteoarthritic inflammatory condition [39, 40]. Since, in the advanced stage of OA, the joint suffers heavy cartilage loss, OA treatment strategies

must evolve to support neocartilage formation within the OA niche.

The present study addresses this challenge through the fabrication of a chemically defined silk-based biomaterial that supports the regeneration of articular cartilage within a severe OA-afflicted rat joint. We hypothesized that a single biomaterial construct could provide adequate mechanical resilience while simultaneously upregulating pro-articular cartilage Wnt/β-catenin signaling [32, 33, 35] and downregulate the pro-ossification BMP signaling pathway as well as impart immunomodulatory effects to the surrounding OA niche. The sustained anti-osteoarthritic conditions can be achieved through covalent conjugation of BMP inhibitor, LDN-193189, into the SF-G bioink that can aid in articular cartilage regeneration in the OA knee joint, while simultaneously maintaining the hyaline nature of neocartilage. Therefore, while designing this study, we raised the following questions:

- Can chemically decorated SF-G material support in vitro chondrogenesis?
- When implanted in a full-thickness defect of an osteoarthritic rat knee, will this chemically defined SF-G biomaterial support neo-cartilage formation by inhibiting the BMP signaling pathway?
- Will the new cartilage regenerate within the full-thickness defect of an OA rat model retain hyaline cartilage characteristics, inhibit chondrocyte hypertrophy and hypersecretion, and maintain a stable articular cartilage phenotype?
- Can this new SF-G biomaterial modulate the inflammatory characteristics of the surrounding OA cartilage tissue niche?

The constructs were implanted within a full-thickness cartilage defect in the rat femoral trochlear groove, which had already been subjected to anterior cruciate ligament transection (ACLT) for the surgical induction of OA. Post-harvest, the knee joints were assessed for cartilage regeneration using radiological, histological, and molecular methods. Results from our study demonstrated successful neo-articular cartilage regeneration in the SF-G-LDN-193189 group at 4 months post-implantation within the defect site of the OA rat model, corroborating our hypothesis.

2 | Results

2.1 | Evaluation of Physicochemical Properties and Mechanical Resilience of the LDN-193189 Conjugated 3D Printed SF-G Constructs

The physicochemical and mechanical properties of the SF-G-LDN-193189 3D-printed construct were first evaluated in vitro to assess its potential to regenerate neo-cartilage under in vivo OA conditions (Figure 1a). Figure 1b demonstrates a digital and corresponding microscopic image of a 6-layered 3D bioprinted chemically-modified SF-G constructs embedded with rat bone marrow-derived mesenchymal stem cells (rat BMSCs) with an inter-filament pore distance of 1.5 mm, indicating adequate printability of the chemically decorated SF-G bioink. The degradation rate of the 3D bioprinted SF-G-based constructs was evaluated to determine their structural stability and resilience under osteoarthritic conditions in the knee joint. The degradation rate of the LDN-193189-conjugated SF-G bioprinted constructs showed a 65% mass fraction remnant on day 14, corresponding to a 35% degradation of the SF-G constructs when incubated in PBS at 37°C for 14 days (Figure 1c,d). The swelling analysis of the SF-G constructs showed an increasing trend from day 1 to day 14, with a 10% increase on day 1 to an 80% increase on day 14, comparable to SF-G-LDN-193189 (Figure 1e,f). Such water-imbibing characteristics correspond to the construct's behavior in the presence of synovial fluid, blood, and other interstitial fluids within the knee joint. The mechanical properties of the implanted construct were evaluated as a function of thickness loss by applying a specified load for a given period. The compressibility, recoverability, and load exhibited an interdependent relationship, with the highest compressibility observed at the highest load (500 gf/cm^2). In contrast, the highest recoverability was observed for the lower load ranges on the construct (20–100 gf/cm^2) (Figure 1g–i and Figure S1). Such mechanical properties will enable the constructs to withstand the compression forces when implanted in the knee joints of osteoarthritic rat models.

Atomic Force Microscopy (AFM) analysis provided direct information on nanoscale topography, indentation depth profiles, and localized mechanical heterogeneity across the samples. The SF-G-CyCl-LDN group (Figure 1j i–iii) showed the most pronounced alterations in topography and nanoscale mechanics. The height sensor map revealed an overall height range (−14.7 to +17.3 μm), demonstrating a controlled and optimal average roughness compared to random irregularity. The PeakForce error distribution spans from −2.9 to +2.6 nN, suggesting minimal heterogeneity in stiffness and an optimal load distribution across the surface. However, the SF-G-LDN (Figure 1j iv–vi) (−1.8 to +2.6 μm) and SF-G (Figure 1j vii–ix) (−1.3 to +6.1 μm) control groups demonstrated relatively smooth, weakly structured, gradient-driven surface topologies with moderate height variation. The PeakForce error map revealed an irregular, broader distribution of −4.2 to +2.1 nN (SF-G-LDN) and −3.6 to +3.7 nN (SF-G), respectively, demonstrating non-uniform nanoscale interactions.

2.2 | The 3D Bioprinted Chemically Modified SF-G Construct Promoted In Vitro Chondrogenesis of the Encapsulated Rat BMSCs

Next, we investigated the in vitro chondrogenesis potential of the 3D bioprinted chemically modified SF-G construct with encapsulated rat BMSCs. A proof-of-concept cytocompatibility assessment demonstrated no significant difference in cellular proliferation (measured as a function of Alamar blue intensity) between chemically-modified and unmodified SF-G constructs, indicating the cell-friendly characteristics of the chemical modification (Figure S2). Compared to the SF-G control, an enhanced expression of collagen type II (ColII) (Figure 2a) with a downregulated expression of the hypertrophic ColX (Figure 2b) protein was observed by immunofluorescence analysis in the 3D bioprinted SF-G-LDN-193189 group at day 28. The qPCR analysis of the ECM marker gene collagen type II alpha chain (COL2A1) and SRY box transcription factor 9 (SOX9) demonstrated a 5-times ($p < 0.05$) and 1.6-times ($p < 0.05$) higher expression in the SF-

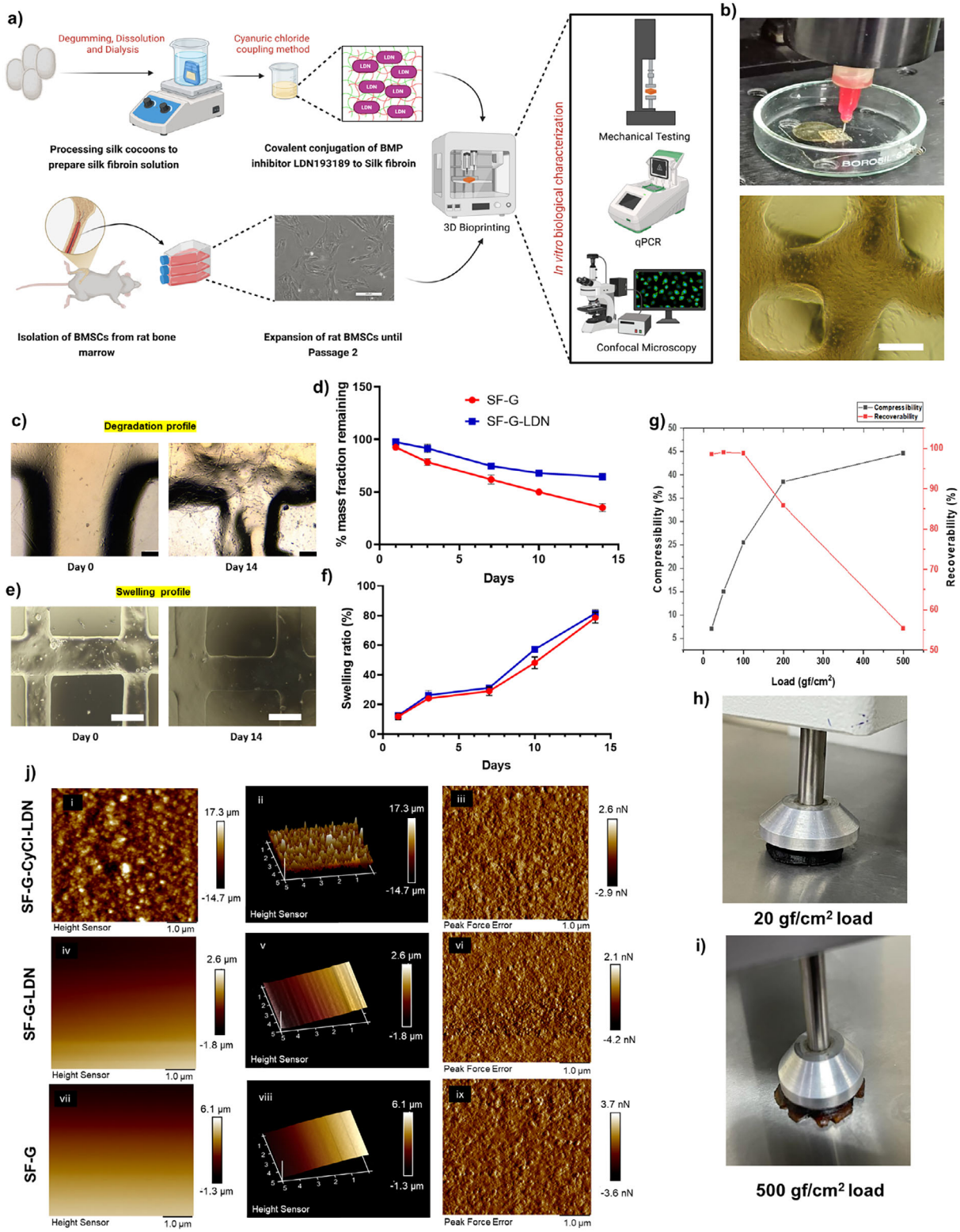

FIGURE 1 | Physicochemical characterization of the chemically modified SF-G constructs (a) Schematic representation of in vitro physical, mechanical and biological characterization of 3D bioprinted LDN-193189 SF-G constructs, (b) Representative images of 3D bioprinted chemically modified SF-G constructs with rat BMSCs (Scale bar: 200 µm), (c) Representative microscopic image of 3D bioprinted SF-G-LDN constructs before (day 1) and after (day 14) degradation (Scale bar: 100 µm), (d) Comparative degradation profile of SF-G constructs with and without LDN conjugation ($n = 3$), (e) Representative microscopic image of 3D bioprinted SF-G-LDN constructs before (day 1) and after (day 14) swelling, (Scale bar: 500 µm) (f) Comparative swelling profile of SF-G constructs with and without LDN conjugation ($n = 3$), (g–i) Compressibility and recoverability of LDN-conjugated 3D bioprinted SF-G constructs ($n = 3$) immediately following enzymatic crosslinking with mushroom tyrosinase (same day as construct preparation) and (j) AFM analysis of chemically modified and unmodified SF-G films.

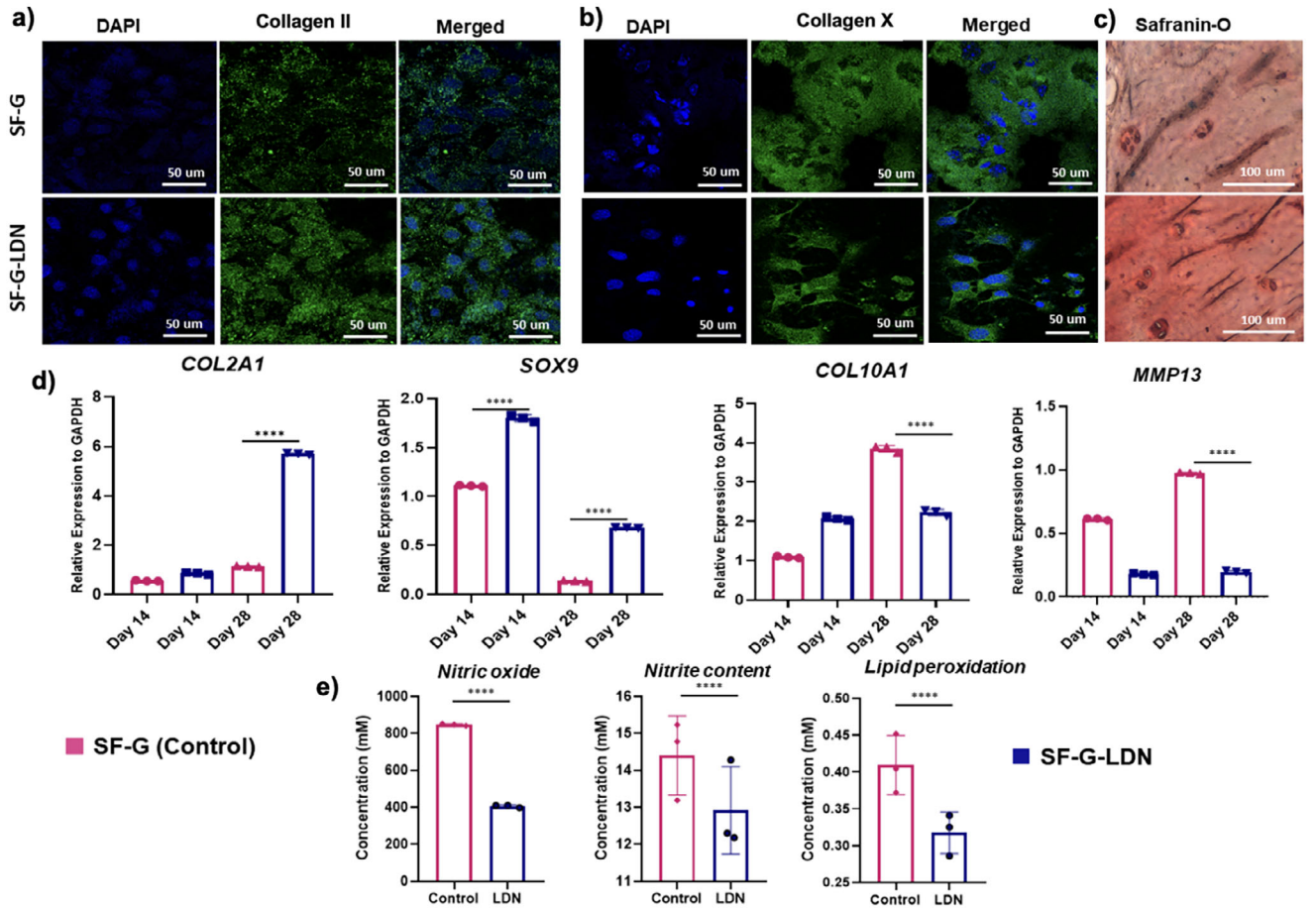

FIGURE 2 | In vitro biological characterization of the 3D bioprinted SF-G-LDN-193189 constructs. (a) Immunofluorescence analysis of collagen II expression in LDN-193189-conjugated and control 3D bioprinted SF-G constructs, (b) Immunofluorescence analysis of collagen X expression in LDN-193189-conjugated and control 3D bioprinted SF-G constructs, (c) Safranin O staining in LDN-193189-conjugated and control 3D bioprinted SF-G constructs, (d) Gene expression analysis of chondrogenic and hypertrophic marker genes in LDN-193189-conjugated and control 3D bioprinted SF-G constructs ($n = 3$), and (e) Biochemical estimation in LDN-193189-conjugated and control 3D bioprinted SF-G constructs ($n = 3$) (*$p < 0.05$, **$p < 0.01$ and ***$p < 0.001$).

G-LDN-193189 group than in the SF-G control group at day 28. Within the LDN-193189 conjugated group, COL2A1 expression was 6.6-fold higher from day 14 to day 28, indicating adequate deposition of the collagen type II matrix and chondrogenesis. The expression levels of the hypertrophic marker genes COL10A1 and MMP-13 were downregulated in the LDN-193189-conjugated group compared to the control group on day 28 (Figure 2d). This was further supported by Safranin O staining (Figure 2c) and by inflammatory mediator measurements, which showed enhanced sGAG deposition and decreased levels of nitrite, nitric oxide, and lipid peroxidation in the LDN-193189-conjugated SF-G group at day 28 compared to the control (Figure 2e).

2.3 | LDN-193189-Conjugated SF-G Construct Encouraged Cartilage Repair and Proteoglycan Restoration Within Full-Thickness Cartilage Defects in the OA Rat Knee Joint

Furthermore, to validate the chondrogenic potential of the 3D printed SF-G-LDN-193189 construct in vivo under OA conditions, we implanted these constructs into critical-sized cartilage defects in rat knee articular cartilage after 28 days of ACL transection (Figure 3a). The knee joints were harvested at two different time points (2 months and 4 months) post-implantation of the modified and unmodified SF-G constructs. Gross morphological examination revealed no obvious healing in any of the groups 2 months post-implantation. Compared to the No construct group and only SF-G constructs (the group representing the SF-G construct lacking LDN-193189), signs of neocartilage formation were visible in the SF-G-LDN-193189 group 4 months post-implantation in the defect site (Figure 3b i–viii).

A μCT scanning technique was utilized to analyze the presence of osteophyte formation at the defect site. Fewer osteophytes were observed in the SF-G-LDN-193189-implanted constructs compared with the other groups. In the group containing the implanted SF-G-LDN-193189 construct, the damage is restricted to the defect site only, both in post-implantation 2-month and 4-month harvested samples, whereas, in the No construct group or in the SF-G group, the defect was widened, exposing the subchondral bone beneath it, indicative of the degraded articular cartilage in the regions surrounding the defect site. (Figure 3c i–viii).

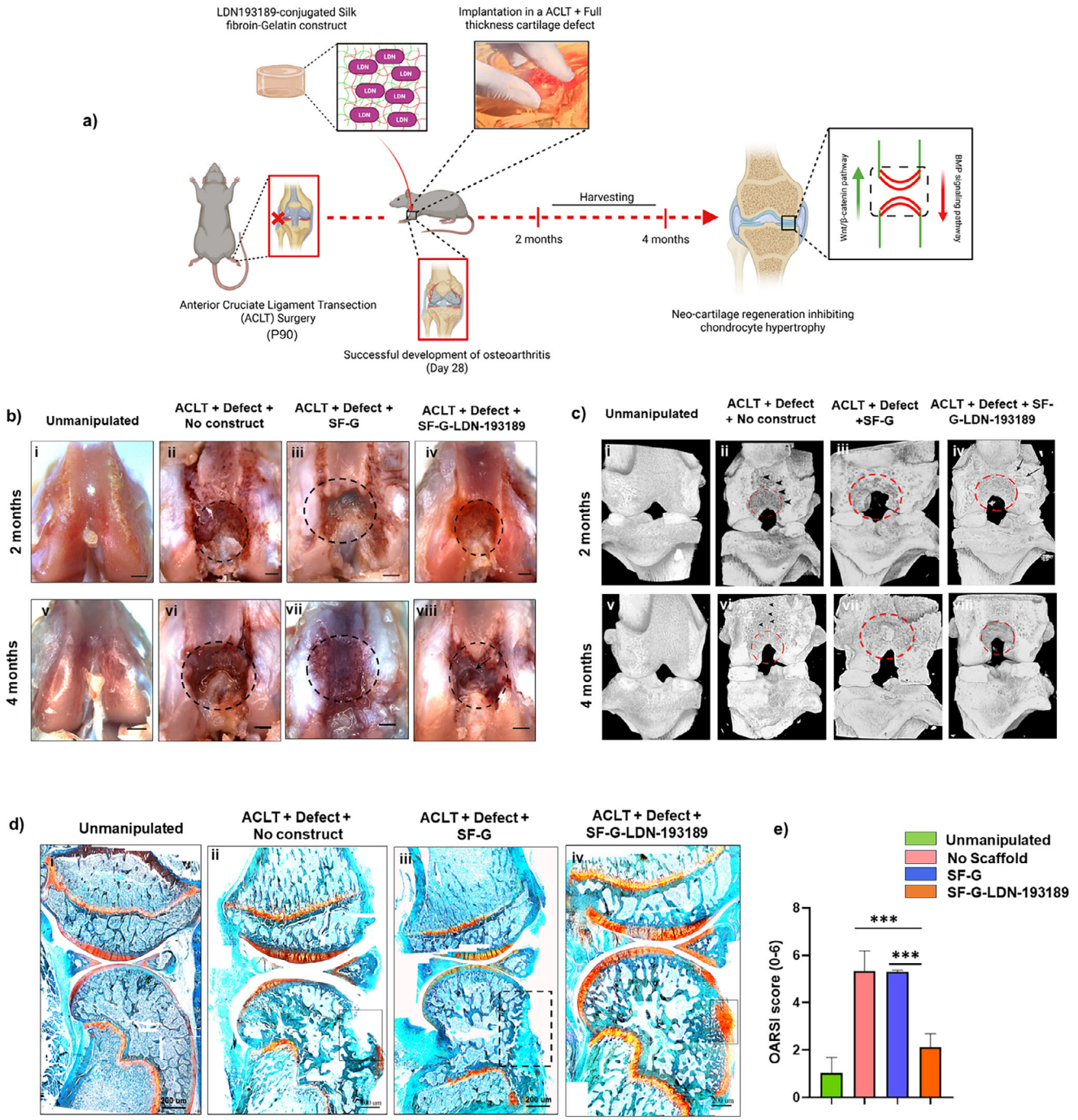

FIGURE 3 | LDN-193189-conjugated SF-G constructs promote site-specific cartilage repair and proteoglycan restoration within cartilage defects in the rat OA knee joint. (a) Schematic representation of the experimental strategy for implantation of SF-G-LDN-193189 conjugated constructs in a full-thickness cartilage defect model post-ACLT day 28. (b) (i–viii): Gross morphology of the knee joint depicting various experimental groups post 2 months and 4 months implantation (Scale bar: 1 mm; $n = 4$), (c) (i–viii): 3D rendering volumetric micro-CT scanning of knee joints depicting experimental groups, (d) (i–iv): Histopathological (Safranin O/Fast Green) staining of post-implantation 4 months (Scale bar: 200 μm; $n = 4$)., (e) Blind OARSI scoring, Brown-Forsythe test (ANOVA), and Tukey's multiple comparison tests were performed to assess the significance and simultaneous comparison of the multiple sets. We compared the means of Unmanipulated vs. ACLT + Defect + No construct group, $p = 0.0001$(***); ACLT + Defect + No construct group vs. ACLT + Defect + SF-G-LDN-193189, $p = 0.0009$(***); and ACLT + Defect + SF-G vs. ACLT + Defect + SF-G-LDN-193189, $p = 0.0009$(***).

Moreover, we confirmed the presence of sulfated proteoglycans (sGAGs) using classical histological methods. We performed Safranin-O staining on tissue sections obtained from all experimental groups after 4 months of implantation (Figure 3d). Compared to the No construct (Figure 3d ii) and SF-G implanted (Figure 3d iii) samples, a deep-red Safranin O staining was observed in the defect site of SF-G-LDN-193189 (Figure 3d iv) group, which was comparable to the unmanipulated group (Figure 3d i). Further, the significantly lower OARSI score for the SF-G-LDN-193189 group confirms the presence of better cartilage

integrity as compared to the No construct or the SF-G group (p = 0.001) (Figure 3e).

2.4 | Sustained Inhibition of BMP Cascade by LDN-193189-Conjugated 3D Printed Constructs Promotes Regeneration of Hyaline Cartilage Within the Full-Thickness Defects in the Rat OA Knee Joint

To evaluate the functional activity of LDN-193189 released from the SF-G-LDN-193189 constructs, the 3D printed constructs were incubated in DMEM supplemented with 10% FBS on a rocker at room temperature for 1, 4, and 7 days. Conditioned media were collected at each time point and applied to serum-starved BRITER cells, a BMP-responsive immortalized osteoblast reporter line carrying a dual luciferase construct (pGL4.28-BRE-FFLuc-IRES-RRLuc) that quantifies BMP signaling via firefly luciferase activity normalized to Renilla luciferase (Figure S4) [41]. Cells were treated with recombinant BMP2 alone (control), BMP2 with 200 nM LDN-193189, or BMP2 with media containing released LDN-193189 (Table S1). After 6 h of treatment, luciferase activity was measured using a dual-luciferase assay. The results demonstrated a significant reduction in BMP-induced luciferase activity in cells treated with conditioned media collected on days 4–7, compared with control cells exposed to BMP2 alone. This indicates that the LDN-193189 released from the construct remained stable and biologically active over this time period, effectively inhibiting BMP signaling as measured by the dual luciferase reporter assay (Figure 4a i–iii). Additionally, the inhibition of BMP signaling by the SF-G-LDN-193189 group in the rat knee joint was confirmed by pSMAD1/5/9 immunohistochemistry. Compared to the No construct (Figure 4b ii) and SF-G implanted (Figure 4b iii) specimens, we observed downregulated pSMAD1/5/9 expression in the defect site of the SF-G-LDN-193189 group (Figure 4b iv), comparable to the unmanipulated ones (Figure 4b i).

2.5 | LDN-193189 Conjugated 3D Printed Constructs Promote Hyaline Cartilage Regeneration and Suppress Hypertrophy and Fibrocartilage Formation Within Full-Thickness Cartilage Defects in the Rat OA Knee Joint

Finally, we investigated whether the SF-G-LDN-193189 construct could induce neocartilage formation in a rat femoral trochlear cartilage defect already affected by OA. To address this objective, we implanted the SF-G-LDN-193189 constructs with corresponding controls. Post 2-month implantation, no ColII expression was observed in the No construct or any of the construct-implanted groups. Further, we observed the absence of ColX expression in the LDN-193189 conjugated SF-G implanted group only, as compared to the No construct or SF-G without LDN-193189 specimens (Figure 5a i–iv, b i–iv).

At 2 months post-implantation, evidence of cell homing from the surrounding tissue into the defect site was observed in the specimens implanted with SF-G (Figure 5a iii) or SF-G-LDN-193189 (Figure 5a iv) and even in the No construct group (Figure 5a ii). However, 4 months post-implantation, only in the SF-G-LDN-193189 group (Figure 5a viii) was strong ColII expression observed, suggesting that this construct enables migrated cells to survive and differentiate into healthy chondrocytes (Figure 5a viii). Further, we did not observe a significant level of ColX expression in the regenerated cartilage (Figure 5b vii). It should be noted that comparing the quantitative expression levels of different markers between the SF-G-LDN-193189 group and the No construct or SF-G group was not possible, as very few cells, if any, were present within the defect site in these two groups.

The expression profile of ColI in the tissue sections from all the experimental groups was examined to confirm the absence of fibrocartilage, which consists of a mixture of ColI and ColII. We observed that in the 4 months post-implantation, the SF-G group lacking LDN-193189 showed ColI expression in cells that migrated into the defect site (Figure 5c vii). In contrast, in the 2 months post-implantation of the SF-G group lacking LDN-193189 (Figure 5c iii) or in samples where no construct was implanted, we observed that although no tissue regenerated at the defect site, the subchondral bone beneath was exposed, as evidenced by ColI immunoreactivity on its surface. (Figure 5c ii,iii,vi). In contrast, we observed a low level of ColI expression 2 months post-implantation at the surface of the defect site where SF-G-LDN-193189 was implanted (Figure 5c iv), but cells within the defect site did not express ColI. Moreover, in the 4 months post-implantation samples, no ColI expression was observed either on the surface or in the interior of the defect site (Figure 5c viii). It is possible that the cells that migrated to the surface of the SF-G-LDN-193189 implanted post-2 months initially formed some fibrocartilage; however, by 4 months, more cells infiltrated the defect site from the bone marrow, replacing the ColI-positive cells with healthy articular chondrocytes.

2.6 | LDN-193189-Conjugated 3D Printed Constructs Attenuate Inflammatory Pathways to Create a Pro-Regenerative Niche Within Cartilage Defects in the Rat OA Knee Joint

Earlier, it was demonstrated that intra-articular injection of LDN-193189 in surgically induced OA joints prevented inflammation and the onset of hypertrophy [20]. Therefore, the presence of the inflammatory marker Nuclear Factor kappa B (NFκB) was investigated in all the experimental groups. NFκB serves as a pivotal mediator of the inflammatory response in the joint, facilitating cartilage degradation and maintaining bone homeostasis [42]. Compared to the No construct group (Figure 6a ii,ii',vi,vi') or SF-G implanted group (Figure 6a iii,iii',vii,vii'), where significant NFκB expression was observed at the defect site post 2 months and 4 months implantation, no detectable NFκB expression was observed in the newly formed tissue at the defect site in the SF-G-LDN-193189 group (Figure 6a iv,iv',viii,viii'), similar to the unmanipulated group (Figure 6a i,i',v,v'). Absence of NFκB expression in the SF-G-LDN-193189 group indicates the presence of a favorable environment for cartilage regeneration.

3 | Discussion

Strategies to regenerate articular cartilage tissue have been adopted by researchers worldwide, utilizing a varying combination of biomaterials (alginate [7], chitosan [43], collagen [44], silk

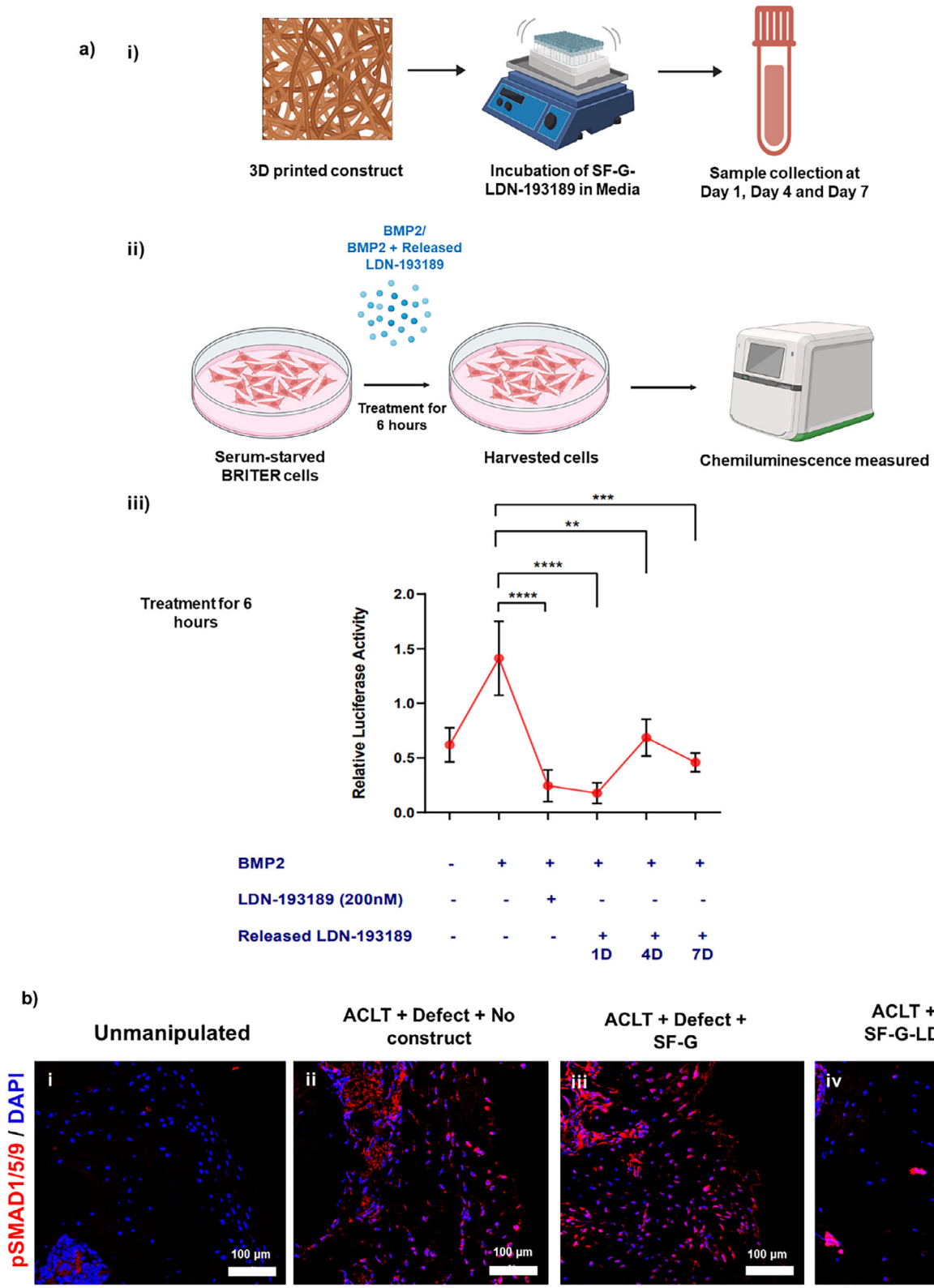

FIGURE 4 | LDN-193189-conjugated 3D printed constructs inhibited the BMP signaling pathway in cartilage defects within the rat OA knee joint. (a) (i–iii) Dual Luciferase reporter assay (BRITER), ($n = 3$); BMP2 vs. BMP2 +LDN-193189 (200 nM) p-value < 0.0001, BMP2 vs. BMP2 + LDN-193189 1D (media collected after 1day LDN-193189 release) p-value < 0.0001, BMP2 + LDN-193189 4D (media collected after 4 days LDN-193189 release) p-value = 0.0041, BMP2 + LDN-193189 7D (media collected after 7 days LDN-193189 release) p-value 0.0004; (b) (i–iv): pSMAD1/5/9 immunostaining of rat knee joint post 4 months implantation for different experimental groups. (Scale:100 µm; $n = 4$).

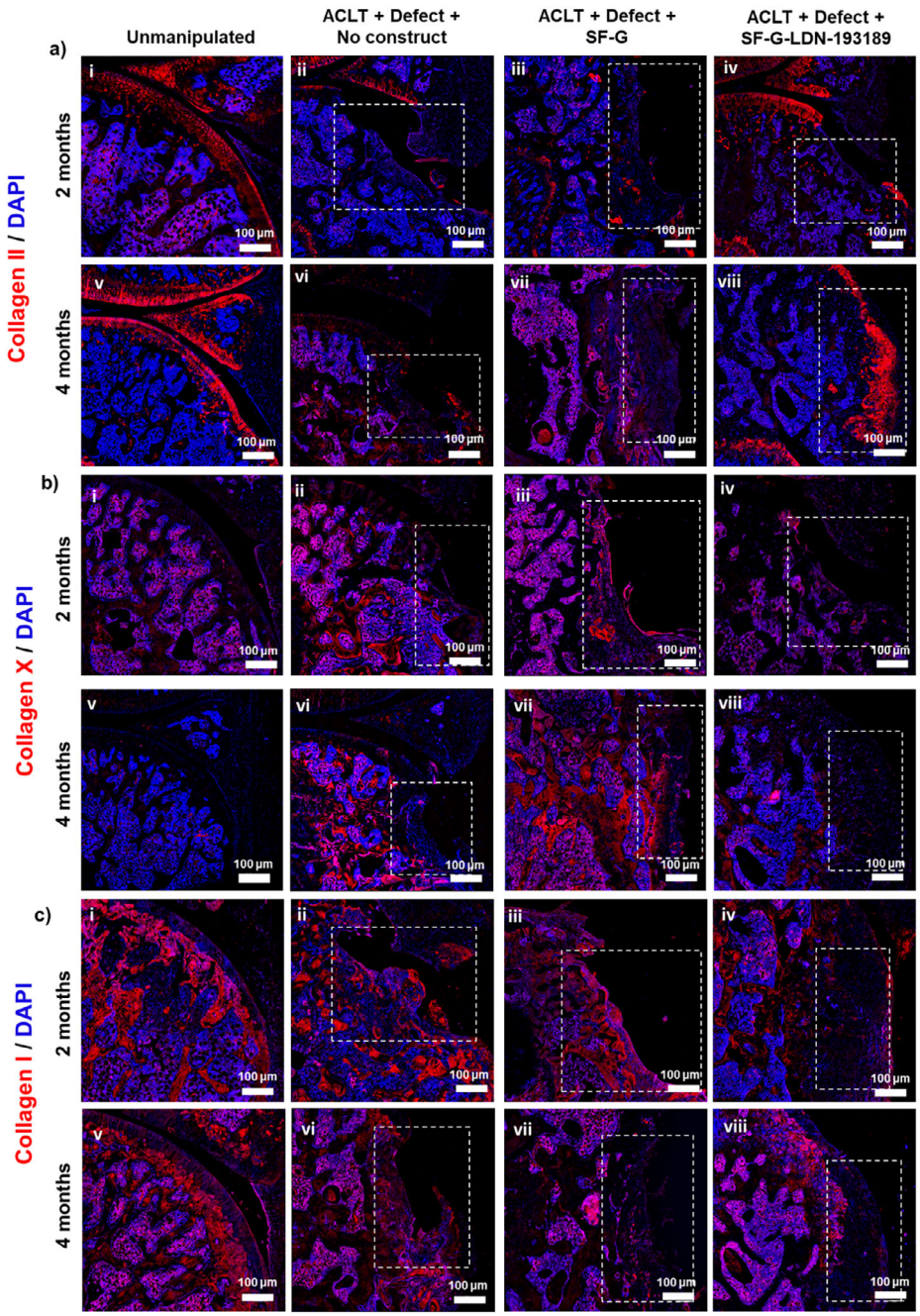

FIGURE 5 | LDN-193189-conjugated 3D printed constructs promote regeneration of hyaline cartilage and suppress hypertrophy in cartilage defects in the rat OA knee joint. (a) (i–iv) ColII immunostaining of rat knee joint of post 2-months implantation and (a) (v–viii) post 4-months implantation for different experimental groups (Scale bar: 100 µm; $n = 4$), (b) (i–iv) ColX immunostaining of rat knee joint of post 2-months implantation and (b) (v–viii) post 4-months implantation for different experimental groups (Scale bar: 100 µm; $n = 4$), (c) (i–iv) ColI immunostaining of rat knee joint of post 2-months and (c) (v–viii) post 4-months implantation for different experimental groups (Scale bar: 100 µm; $n = 4$). White boxes mark the site of the created defect area.

[45], etc.) and cell types (articular chondrocytes [46], adipose-derived stem cells [47], or bone marrow-derived mesenchymal stem cells [31]). Our research group has also investigated various hypotheses concerning chondrogenic differentiation, including a comparative chondrogenesis profile between hBMSCs and articular chondrocytes [31], 3D spheroids vs. single cells embedded in SF-G bioink [31], the role of TGFβ isoforms (TGFβ1 [32] and TGFβ3 [33]) in chondrogenesis, and the anti-inflammatory M2 macrophage-mediated mitigation of OA [12]. We have also demonstrated the superior role of covalently conjugating chondrogenic growth factors into our matrix over their exogenous supplementation in promoting the chondrogenic differentiation of human bone marrow stromal cells (hBMSCs) [9]. Despite advances in tissue engineering, a lack of understanding of the signaling mechanisms underlying embryonic cartilage development and the onset of chondrocyte hypertrophy in implanted cartilage grafts has rendered these approaches futile for the past 40 years. The present study demonstrated the development of a

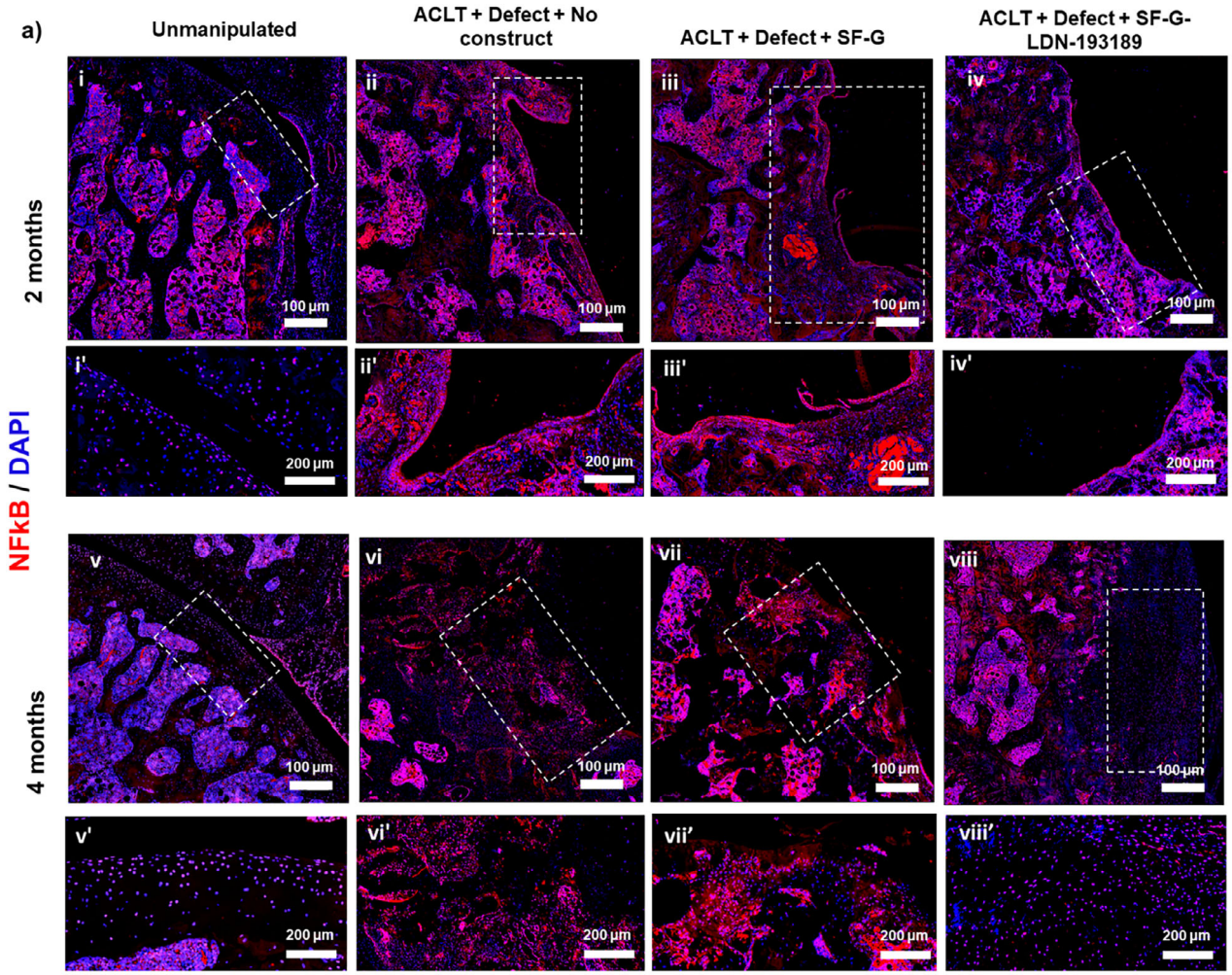

FIGURE 6 | LDN-193189 Conjugated 3D printed constructs attenuate inflammatory pathways to create a pro-regenerative niche in cartilage defects within the rat OA knee joint. (a) (i–iv) NFκB immunostaining of the rat knee joint after 2 months of implantation, (Scale bar:100 μm), and (i'–iv') Magnified cross-section of the defect site in (i–iv), (Scale bar: 200 μm), (b) (v–viii) NFκB immunostaining of the rat knee joint after 4 months of implantation for different experimental groups, (Scale bar: 100 μm), (v'–viii') Magnified cross-section of the defect site, (Scale bar: 200 μm; $n = 4$). White dashed boxes mark the created defect site; (i'–viii') are the magnified cross-sections of (i–viii).

novel chemically modified SF-G construct for the regeneration of articular cartilage in an osteoarthritic knee joint. The BMP signaling pathway plays a significant role in the progression of OA [48]. Furthermore, it has been reported that surgical induction of OA upregulates the BMP signaling cascade in articular chondrocytes, leading to increased proliferation, a phenomenon undetectable in healthy tissue. Additionally, the Wnt signaling cascade is a key regulator of articular cartilage phenotype maintenance and regeneration [49]. However, an imbalance in Wnt activation can also potentiate OA progression [50]. Therefore, we adopted a strategy based on the principles of developmental biology to induce articular cartilage regeneration in an in vivo OA microenvironment by simultaneously inhibiting the BMP signaling pathway through the covalent conjugation of the BMP inhibitor LDN-193189 and the inherent upregulation of the Wnt signaling cascade using the SF-G bioink [32, 33, 35].

To validate our first hypothesis regarding the physicochemical characterization and in vitro chondrogenic potential of our chemically decorated 3D bioprinted SF-G constructs, we have employed detailed biological and material characterization techniques. The SF-G polymer blend has been used as a versatile bioink for cartilage tissue engineering applications [31, 51]. Small-molecule regulators play a significant role in governing cartilage tissue morphogenesis by modulating associated cell signaling cascades [21, 34]. Therefore, LDN-193189 was covalently conjugated to our SF biomaterial prior to 3D bioprinting using the cyanuric chloride (CyCl) method to increase the temporal bioavailability of the small molecule to the embedded cells, which would otherwise require frequent replenishment due to shorter half-life, making the culture process expensive and cumbersome. Therefore, this covalent conjugation strategy will be beneficial for the in vivo implantation by not only inhibiting hypertrophy via BMP pathway inhibition but also temporally priming the infiltrating cells to differentiate into articular chondrocytes. The chemically modified silk was further supplemented with gelatin to impart additional cytocompatibility and shear-thinning properties before 3D bioprinting [26]. Such covalent attachment, as confirmed by ATR-FTIR and molecular modeling, ensured a sustained release profile after implantation of the constructs into full-thickness cartilage defect sites [35]. To ensure that these constructs support chondrogenesis, chemically modified SF-G

constructs were 3D bioprinted with rat BMSCs and then incubated in chondrogenic medium for 28 days. The 3D bioprinted cell-laden SF-G constructs for in vitro chondrogenesis evaluation exhibited a 6-layered structure with an inter-filament pore dimension of 1.5 mm, ensuring adequate pore interconnectivity and nutrient transfer. The incorporation of rat BMSCs at a cell density of 1 million cells/mL into the SF-G bioink did not alter the rheological and printability properties of the bioink [52]. The chemically modified 3D bioprinted SF-G constructs also demonstrated enhanced stability compared to the unmodified SF-G group, with a 65% remaining mass fraction at day 14, possibly due to an increase in beta-sheet content resulting from CyCl chemical modification, which rendered increased structural integrity [35]. The increased structural stability of the chemically modified SF-G constructs was further corroborated by mechanical testing, which showed approximately 50% compressibility under a high compression force of 500 gf/cm^2. Thus, the developed 3D bioprinted SF-G-LDN-193189 hydrogel demonstrated a compressive tolerance of ~50 kPa with high structural recoverability (~10 kPa), indicating permissiveness to higher mechanical deformation without complete failure. Although the mechanical strength value is comparatively lower than the compressive modulus of native human articular cartilage (240–1000 kPa) [53], typical hydrogel constructs tend to exhibit one order of magnitude lower modulus values than native cartilage, designed primarily to allow chondrocyte infiltration and cartilage-specific ECM secretion [53].However, the induction of β-sheet crystallization within the chemically modified SF-G matrices following implantation and exposure to physiological conditions (temperature, pH, body fluids) [54, 55] can enhance structural stability [56] and further contribute to construct integration at the defect site. The mechanical variability is further evident in the AFM data of the SF-G-CyCl-LDN group, demonstrating controlled roughness and an optimal force distribution across the biomaterial surface. Such behavior is consistent with the synergistic effects of covalently conjugating LDN-193189 to CyCl, which significantly increase the β-sheet content, likely inducing microstructural rearrangements and localized stiffening zones within the fibroin matrix [35] compared to the direct LDN encapsulation to the SF-G matrix. Therefore, 3D bioprinting of the chemically decorated SF-G constructs provided additional advantages over conventional scaffolding techniques by providing spatiotemporal cues [26] and topological signals (a mechanically stable porous structure), along with increased bioavailability of the small molecule within the construct, to support the successful in vitro chondrogenic differentiation of encapsulated rat BMSCs. Spatiotemporal cues, such as dynamic stimulus-based bioprinting approaches, significantly upregulate articular cartilage-specific gene expression, with enhanced COL-II and glycosaminoglycan secretion compared to static SF-G constructs [57]. In our study, the 3D bioprinting technique with encapsulated rat BMSCs promoted shear-induced alignment of cells along the printing direction, thereby enabling homogeneous cellular distribution and efficient nutrient exchange within the 3D constructs [26]. The shear force further allowed the alignment of collagen fibres along the surface of the 3D construct [58] with the elongated cellular morphology, similar to the native cartilage superficial zone. Additionally, the sequential release of the covalently tethered BMP inhibitor, LDN-193189, from the SF-G constructs [35] established a small-molecule BMP inhibitor gradient to maintain a perfect balance between the prevalence of the pro-chondrogenic BMP pathway to stimulate chondrogenesis [59, 60] and the inhibition of the pro-hypertrophic BMP cascade to mitigate chondrocyte hypertrophy [20]. In vitro biological characterization results with BMSCs confirmed the chondrogenesis and inhibition of chondrocyte hypertrophy by our chemically decorated 3D bioprinted SF-G constructs, which exhibited enhanced expression of cartilage-specific biomarkers (COL2A1, SOX9) and downregulation of osteogenic and hypertrophic markers (MMP13, COL10A1). However, a decrease in SOX9 expression at day 28 can be attributed to the successful chondrogenic differentiation, as evident by elevated expression of COL2A1, a late-stage chondrogenic marker whose expression is strongly regulated by the enhanced expression of SOX9 at day 14 [61].

Studies have reported the regeneration of articular cartilage in full-thickness cartilage defects using different standalone or composite hydrogel combinations like chitosan/decellularized matrix composite, silk fibroin/collagen, or silk fibroin/gelatin hydrogel systems with or without cells [62–64]. Although healing has been observed in all the samples, disadvantages associated with injectable scaffolds compared to implantable ones, a lack of understanding of the quality of the neo-cartilage formed, and a need for mechanistic insights into hyaline cartilage formation remain major roadblocks. Conventional defect models often demonstrate localized hyaline cartilage repair; however, they fail to replicate the multifactorial challenges of OA. Hence, evaluating neo-cartilage formation within an OA knee joint offers a more rigorous platform to assess both regenerative efficacy and the biomaterial's capacity to manage inflammation and chondrocyte hypertrophy. Therefore, from the positive results of our in vitro analysis, the LDN-193189-conjugated SF-G constructs were implanted in a full-thickness cartilage defect within the knee joint of an OA rat induced by ACLT.

To address our next hypotheses, the knee joints harvested 2 months and 4 months after implantation were extensively characterized for articular cartilage-specific matrix production and inhibition of hypertrophy, as well as fibrocartilage formation and inflammation. As previously reported, in situ inhibition of BMP signaling provides protection against surgically induced OA, restoring articular cartilage tissue within the inflammatory microenvironment [20]. Thus, it was hypothesized that the simultaneous inhibition of the BMP signaling pathway through the sustained release of the LDN-193189 and the upregulation of the Wnt signaling pathway by SF-G biomaterial [32, 33, 35] would aid cartilage regeneration in an OA joint. Our results corroborated our hypothesis, showing dense ECM production (as indicated by Safranin O) and intense ColII expression in the LDN-193189-conjugated implanted constructs compared with the No construct and SF-G specimens. ColII is a typical biomarker for hyaline cartilage, making up almost 90% of the total articular cartilage matrix composition [65]. Hence, the dense ColII staining in our SF-G-LDN-193189 group, compared to the SF-G and No construct groups, signifies the formation of a hyaline cartilage phenotype in the defect area, thereby indicating a direct correlation between BMP pathway inhibition and articular cartilage formation. This is in line with the results by Franco et al. that demonstrated the pro-chondrogenic role of BMP signaling inhibition by LDN-193189 treatment in promoting chondrogenic differentiation of BMSCs marked by enhanced ColII, ACAN, and SOX9 expression [66]. Also, the LDN-193189 conjugated constructs depicted a negligible expression of BMP signaling downstream target pSMAD1/5/9

compared to the No construct and SF-G group, indicating the inhibition of the BMP signaling cascade within the OA niche. The results also correlate with the findings from Boergermann et al., demonstrating the LDN-193189-mediated inhibition of smad and non-Smad signaling pathways in C2C12 cells, activated by BMP ligands [67].

The next aim of the research was to investigate whether the small molecule-conjugated SF-G constructs can inhibit the onset of chondrocyte hypertrophy in the newly formed articular cartilage when exposed to the OA milieu. This was examined by immunofluorescence analysis of the key hypertrophic marker ColX in harvested rat knee joints. ColX plays a significant role in the hypertrophic differentiation of chondrocytes, further contributing to bone formation through the endochondral ossification pathway, matrix calcification, and vascularization of the cartilage tissue [68]. Increased levels of ColX protein have also been detected in patient samples with extensive OA, consistent with the expression of ColX, which is typically found only in clustered hypertrophic chondrocytes [69]. Results from our study demonstrated no ColX expression in the SF-G-LDN-193189 group, elucidating the anti-hypertrophic role of the BMP pathway inhibitor LDN-193189. However, the only SF-G constructs showed higher ColX expression than our test group, possibly because they lacked anti-hypertrophic molecules, leading infiltrating cells to convert to a hypertrophic phenotype when exposed to an inflammatory, protease-rich microenvironment for a prolonged period. Under in vitro OA-mimicking conditions, the SF-G only group encapsulated with human BMSCs illustrated a strong tendency toward hypertrophic differentiation, whereas the anti-BMP molecule, LDN-193189-conjugated SF-G constructs showed negligible hypertrophic marker, ColX expression, corroborating the in vivo findings [35].

Furthermore, any sign of fibrocartilage formation in the neo-cartilage tissue was also assessed by the expression of ColI biomarker, which comprises the major component of fibrocartilage matrix and is ideally absent in articular cartilage tissue [70]. A negligible expression of ColI in the 2-month harvested sample that gradually declined with complete suppression of fibrocartilage marker, ColI expression, post 4-month implantation in the SF-G-LDN-193189 group was observed compared to the SF-G and No construct group, where the expression of ColI persisted until 4 months. This denotes the initial formation of fibrocartilage tissue at the defect site within the OA joint niche (2 months), which subsequently converted into a hyaline cartilage phenotype as the magnitude of OA-related factors in the surrounding microenvironment gradually declined (4 months).

Lastly, we evaluated whether our SF-G-LDN-193189 constructs can also inhibit inflammation within the joint defect site when implanted. Chronic inflammation plays a key role in the pathological progression of OA, which is highly regulated by the NF-κB pathway. The activation of the NF-κB cascade stimulates the release of inflammatory cytokines like IL-6, IL-1β, and cyclooxygenase 2 (COX2), causing extensive ECM degradation and hypertrophic differentiation of the resident or infiltrating cartilage-specific cells [71]. The SF-G-LDN-193189 group completely inhibited the activation of the NF-κB pathway with no expression of NF-κB marker genes in the 4-month harvested knee joint samples. Therefore, our chemically modified SF-G-LDN-193189 construct not only promoted hyaline cartilage regeneration but also inhibited inflammation within the defect site in an OA niche. This is in line with the findings from Jaswal et al., where subsequent LDN-193189 injections attenuated inflammation in ACLT-induced mouse models marked by decreased expression levels of IL-1β, TNF-α, and NF-κB, respectively [20]. However, challenges concerning the shorter half-lives of these small molecules mean that our covalent conjugation approach to the SF-G biomaterial would be beneficial for long-term chondroprotective effects in a chronic inflammatory OA microenvironment.

Since our constructs were acellular, the cells observed within the implants must have migrated from surrounding tissues and differentiated into cartilage. In this context, it is worth recalling that the micro-fracture technique relies on the migration of BMSCs that seep out through the arthroscopically created pores [72]. However, the process often leads to the formation of fibrocartilage, possibly because the BMSCs do not encounter a microenvironment that supports the differentiation of articular cartilage [72, 73]. It is conceivable that the SF-G-LDN-193189 constructs provided the cells a chondro-protective (anti-BMP signaling) and chondro-inductive (pro- Wnt/β-catenin) microenvironment [32, 33, 35], allowing them to undergo articular cartilage differentiation.

A possible reason for the lack of healing in the implanted specimens after 2 months is the method of defect formation in the knee joint, which creates a highly inflammatory, hostile environment that prevents neighboring cells from migrating, surviving, and synthesizing cartilage-specific ECM within 2 months. To investigate this possibility, chondrogenically differentiated cell-laden SF-G constructs with and without LDN-193189 were also implanted to assess the role of the construct-resident cells in promoting neo-cartilage generation in vivo. Surprisingly, no cells were detected, nor was any healing observed in the SF-G constructs without LDN-193189 after 2 and 4 months of implantation. However, with the LDN-193189-incorporated cartilage constructs, many cells were detected with no ColII and ColX expression after 2 and 4 months of implantation. Nevertheless, it can be postulated that the presence of LDN-193189 in the constructs protected the cells from the inflammatory environment induced by OA, allowing them to survive but in a dedifferentiated state (Figure S5a–c). Further, it appears that the incorporation of LDN-193189 and the consequent inhibition of inflammatory response in the SF-G-LDN-193189 constructs provided a more hospitable environment for cartilage regeneration. However, it would be equally exciting to observe, with more precise experimental strategies, how the already differentiated BMSCs within a construct contribute to neo-cartilage generation in vivo. Earlier studies by Lee et al. [74] and Hu et al. [44] have demonstrated the regeneration of articular cartilage in surgically induced OA models using SOX gene-transduced fibrin gels or collagen type II scaffolds. However, the absence of any quality assessment of the cartilage type, as well as transcriptomic profiling demonstrating the presence of hypertrophic and fibrocartilage markers, questions the long-term efficacy of these biomaterial-based strategies as a regenerative therapeutic option. In contrast, we used insights from developmental biology to develop a chemically defined construct that can be scaled up and reproduced. The construct we developed in conjunction with microfracture is likely to be an effective disease-modifying therapy for OA.

4 | Conclusion

Our study, for the first time, mechanistically elucidates the potential to regenerate neo-articular cartilage in an OA microenvironment using a defined, chemically modified silk-based biomaterial that can regulate key signaling pathways governing chondrogenesis and OA progression. The SF-G-LDN-193189 group, comprising the BMP signaling pathway inhibitor covalently conjugated with our SF-G bioink, demonstrated successful regeneration of articular cartilage within the full-thickness cartilage defect in an OA rat model. The inhibition of the BMP signaling pathway by our construct not only facilitated neo-cartilage formation but also demonstrated complete inhibition of key OA pathological drivers, including hypertrophic chondrocyte differentiation, fibrocartilage formation, and chronic inflammation. However, subsequent studies will be carried out in higher-order animals, such as dogs, pigs, or humans, to closely simulate articular cartilage regeneration in human load-bearing OA knee joints. Next, we would like to understand how hypertrophic remodeling, "senescent" fibroblasts, and macrophages collaborate to mitigate cartilage remodeling, particularly during aging. Additionally, combining the effects of other small-molecule regulators of OA, such as anti-inflammatory IL-1Ra and pro-chondrogenic growth factor TGF-β3, with LDN-193189 within the SF-G constructs may further promote the formation of high-quality cartilage tissue in a short period. Thus, our advanced tissue engineering strategy, utilizing an FDA-approved silk fibroin biomaterial, would serve as a stepping stone toward developing a permanent regenerative therapy for OA.

5 | Materials and Methods

5.1 | Preparation of Chemically Conjugated SF-G Constructs

The chemically conjugated SF-G constructs were prepared per the previously published protocol [52]. The cut silk cocoons (5 g) were boiled in 0.02 M sodium carbonate (Na_2CO_3) for 20 min to remove sericin. The dried silk fibers were then dissolved in 9.3 M lithium bromide (LiBr) at 60°C for 4 h, followed by dialysis in a Slide-A-Lyzer dialysis cassette against deionized water for 48 h to remove any residual traces of LiBr. The silk fibroin (SF) solution obtained was blended with cyanuric chloride (CyCl) and sodium bicarbonate ($NaHCO_3$) in a 1:1:3 ratio, then reacted at 4°C for 1.5 h. The CyCl-decorated SF solution was then reacted with 100 nM LDN-193189 to form the LDN-193189-conjugated SF solution. The 5% silk solution (SF) was then mixed with ethanol-sterilized 6% gelatin (G), supplemented with 10% Fetal Bovine Serum (FBS) and 10% Minimum Essential Medium (MEM), and incubated at 37°C for 20 min until a clear solution was formed. An 800 U of mushroom tyrosinase was added to the bioink to enable irreversible enzymatic crosslinking [52].

5.2 | Physicochemical Characterization

The swelling study was carried out by incubating the chemically modified and un-modified SF-G constructs in PBS solution at 37°C for 14 days, and the swelling ratio was calculated by the following formula: swelling ratio: $\{(W_W - W_D/ W_D) *100\}$ where W_W corresponds to the wet weight of the constructs, and W_D corresponds to the dry weight of the constructs. The degradation profile of the constructs was evaluated by incubating the chemically modified and unmodified SF-G constructs in PBS and lyophilizing them at the indicated time points. The degradation profile was calculated based on the remaining mass fraction and was given by: $\{(W_M - W_D)/ W_D\} * 100$, where W_M corresponds to the degraded weight of the constructs and W_D corresponds to the dry weight of the constructs. The mechanical properties of the constructs were investigated by calculating their compressibility and recoverability under a given load for a specified period. The compressibility was calculated using the formula: $\{(T_0 - T_F/T_0) *100\}$ where T_0 corresponds to the initial thickness, and T_F corresponds to the final thickness. The recoverability was calculated by: $\{(T_R/T_0) *100\}$ where T_0 corresponds to the initial thickness and T_R corresponds to the recovered thickness.

5.3 | Atomic Force Microscopy (AFM)

Surface topology and mechanical properties of the chemically modified silk biopolymer were evaluated using AFM. Briefly, the CyCl-modified SF-G crosslinked with mushroom tyrosinase, along with the controls, were uniformly cast on glass slides using a RodarICT system to achieve consistent film thickness. The samples were then dried at ambient conditions and subsequently lyophilized for 24 h to obtain stable films. The surface morphology and nanomechanical properties were characterized using a Bruker Dimension Icon atomic force microscope (AFM) operated in PeakForce Tapping mode with MSNL-10 silicon nitride probes (Bruker). Scanning was performed at a rate of 0.996 Hz over areas of 5, 2, and 0.6 μm to capture both global topography and nanoscale structural features. For each sample, height sensor images, three-dimensional reconstructions, and peak force error maps were recorded. All images and indentation data were processed using Nanoscope Analysis 2.0 software (Bruker), applying the 'flatten' function to correct the background slope, and quantitative parameters, including depth profile and surface roughness.

5.4 | In Vitro Biological Characterization

5.4.1 | 3D bioprinting and Chondrogenic Differentiation

The rat BMSCs were isolated according to the protocol described by Yusop et al. [75]. The cells at passage 2 were encapsulated within the LDN-193189-conjugated SF-G bio-ink and 3D bioprinted as Majumder et al. described [35]. Briefly, a 6 mm × 6 mm × 6 mm 3D design was generated using RoboCAD software. The chemically modified SF-G bioink was encapsulated with rat BMSCs at a density of 1 million cells/mL, and the cell-laden bioink was loaded into a sterile barrel connected to a 210 μm nozzle. The printing was carried out at a speed of 1 mm/s and a pressure of 25 PSI. The fabricated constructs were allowed to gel in a cell culture hood for 20 min. The 3D constructs were incubated in chondrogenic medium composed of DMEM/F12 (Gibco) supplemented with 1% antibiotic-antimycotic (Gibco), 1% sodium pyruvate (Gibco), 1% HEPES (Gibco), 1% Insulin-transferrin-selenium (Gibco), 10^{-7} M dexamethasone (Sigma),

and 0.1 mM ascorbic acid-2-phosphate (Sigma) for 28 days with media changes twice a week [31]. The cytocompatibility of the chemically-modified and unmodified SF-G constructs was evaluated using the Alamar blue assay [76]. Briefly, a 10% Alamar blue was added to each well containing 3D bioprinted SF-G-CyCl constructs with rat BMSCs, incubated for 4 h, and the corresponding absorbance was recorded using a UV-spectrophotometer.

5.4.2 | qPCR Analysis

The cells were isolated from the 3D bioprinted constructs (days 14 and 28) by digesting them with 250 µg/mL Protease IV for 20 min. The total RNA was isolated using a RNeasy mini kit column (Qiagen), and the subsequent cDNA was synthesized using a first-strand cDNA synthesis kit (Qiagen). The reaction was performed in triplicate using a SYBR Green Master Mix (Qiagen) kit in a Rotor-Gene Q thermocycler (Qiagen) for the COL2A1, SOX9, COL10A1, and MMP-13 genes (Table S2), with GAPDH as the housekeeping gene for normalization. A day 0 monolayer control was used for calibration. The analysis was carried out using Rotor-Gene Q software [32]. The obtained Ct values were normalized to GAPDH, further calibrated to the day 0 monolayer, and relative expression values were calculated using the 2^-ΔΔCt method.

5.4.3 | Biochemical Estimation

The supernatants of day 28 were used to estimate the total nitric oxide, nitrite content, and lipid peroxidation profile using the respective EZ Assay Nitric Oxide and EZ TBARS assay kit, respectively, following the manufacturer's protocol ($n = 3$) [77].

5.4.4 | Immunofluorescence and Histology Analysis

The respective 3D bioprinted constructs at day 28 were fixed and processed for ColII and ColX protein expression analysis as previously described by Majumder et al. [35]. Briefly, the constructs were incubated with 5 µg/mL anti-collagen II (DSHB) and anti-collagen X (DSHB) primary antibodies overnight at 4°C, followed by washing twice with PBS for 10 min each. The constructs were then incubated with 2 µg/mL Alexa Fluor 488 secondary antibody (Thermo Fisher) for 2 h at RT, followed by washing with PBS twice again for 10 min each. They were then finally treated with 1 µg/mL DAPI (Thermo Fisher) for 15 min and carefully washed with PBS again for 10 min (twice), followed by acquiring the images using a Leica SP5 inverted confocal microscope (Leica Microsystems). The fixed day 28 3D bioprinted constructs were further dehydrated using alcohol gradients and stained with Safranin O and Fast green to evaluate the sGAG deposition. Briefly, the dehydrated constructs were rehydrated in xylene, embedded in paraffin wax, and sectioned (5 µm sections). The samples were then dehydrated with 100% alcohol, stained with 1% Fast green for 5 min, washed quickly with 1% acetic acid (10–15 s), and then stained with 0.1% Safranin O for 5 min. The constructs were then further dehydrated using 95% and 100% ethanol (twice, 2 min each), cleared with xylene, and imaged with a bright-field microscope.

5.4.5 | Dual Luciferase Reporter Assay (BRITER Assay)

The 3D printed constructs were kept in DMEM (Sigma–Aldrich D7777) + 10% FBS (Gibco 10270106) in three different groups (Group 1: 1-day LDN-193189 release, Group 2: 4-day LDN-193189 release, and Group3:7-day LDN-release) on a rocker at room temperature, and media were collected at each endpoint. The culture medium was not changed during this period. BRITER cells were grown till passage 2 in 24-well plates in DMEM +10% FBS [41]. Cultured BRITER cells were serum starved for 6 h (DMEM+1% FBS), after which recombinant 50 ng of BMP2 protein (Sino Biologicals) was added in control vs. BMP2+ (200 nM) LDN-193189 (Sigma SML0559-5MG) and BMP2+ conditioned media (supernatant containing released LDN-193189 from the construct) of day 1, day 4, and day 7 were added to the cells. Again, after 6 h, the cell lysates were collected using a Dual-Luciferase Reporter Assay kit (Promega, Cat. no. E1910), and chemiluminescence was measured using a Glomax Luminometer. Luminescence activity was calculated as a ratio of firefly luciferase and Renilla luciferase ($n = 3$).

5.5 | In Vivo Study Design

5.5.1 | Sample Size

Statistical power calculations were performed using G*Power 3.1 to determine the sample size. The "Resource Equation Approach," as described by Arifin et al. [78], was used to determine the number of animals needed for each experiment. Depending on the impact size, each experimental group consists of 4 animals. A single animal serves as the experimental unit in each experiment.

5.5.2 | Data Exclusion

Animals that perished throughout the experiment were the only ones excluded from the study, even though no outliers were eliminated. At the endpoint of every experiment, data were collected.

5.5.3 | Experimental Design

Controlled laboratory experiments, including in vitro and in vivo studies, were designed to conduct the study. All primary data were collected using qualitative imaging as the primary source and analyzed further using µCT and microscopic imaging.

5.5.4 | Randomization

To avoid randomization, only age-matched animals were used to conduct experiments. Both sexes were included to ensure a gender-unbiased study.

5.5.5 | Animal Study Protocols

All the animals were bred, housed, and cared for in the Central Experimental Animal Facility (CEAF) at the Indian Institute

of Technology, Kanpur, India. Rats were fed feed and water ad libitum, with a 12-h light-dark cycle. According to the guidelines of the CPCSEA, Government of India, all animal research was conducted in accordance with protocol no. IITK/IAEC/2022/1141, approved by the Institutional Animal Ethics Committee. All animals were sacrificed at 6 months or 8 months of age.

5.5.6 | 3D Volumetric Projections of Micro-Computed Tomography (μCT)

CTVol 2.0 was used to create 3D volumetric projections, employing a scanner calibrated to 50 kVp and 200 μA, providing an image resolution of 5.86 μm per pixel. The eXplore Locus GE scanner, located at the Micro-CT Facility of the Indian Institute of Technology, Kanpur, was used to perform, process, and analyze μCT imaging of all tissue samples. The final image, created with Parallax Innovations Micro View 2.5.0- rc15 (2.5.0-3557), had a resolution of 40 μm per pixel.

5.5.7 | Anterior Cruciate Ligament Transection

ACLT surgery was performed in the left hindlimbs of Sprague Dawley rats at P90. We followed the surgical procedure mentioned earlier [20].

5.5.8 | Creating Full-thickness Cartilage Defect and Constructs Implantation

A full-thickness cartilage defect was created in the articular cartilage of the left hindlimb on post-surgery day 28 (Figure S3). Knee joints were exposed by dislocating the patella and holding the joint at a fixed flexion angle. A critical-sized cartilage defect (diameter: 2.3 mm) was created using a 13-G Biopsy Needle. A full-thickness defect was ensured by observing the first evidence of blood. The chemically modified and unmodified cell-free SF-G constructs of the same size were implanted at the defect site and fixed using Reliseal Fibrin Tissue Sealant. The implantation was carried out 24 h after sample preparation and incubation at 37°C. Later, the patella was returned to its original location and sutured with Vicryl 5-0.

5.5.9 | Tissue Processing, Immunohistochemistry, and Classical Histology

Limb tissues were immediately fixed in 4% paraformaldehyde for 24 h at 4°C. Then, the fixed tissues were washed in PBS for 3–4 h twice to remove any trace amount of PFA. Decalcification was performed in 14% EDTA (pH 7.4) at RT for 28 days. After effective decalcification, tissues were dehydrated through a series of alcohol concentrations, with each concentration applied for at least 4 h. Dehydrated tissues were then subjected to xylene and subsequently embedded in paraffin wax to obtain 5-μm-thick sections. Safranin O/ Fast Green staining was performed for histological analysis. Following rehydration, the tissue slices were exposed to Harris hematoxylin (SRL) for 6 h. The sample was then rinsed under running water, immersed in 1% Fast Green stain for 3 min, treated with 1% acetic acid, and subsequently stained for 2 min with 0.5% Safranin O. The tissues were then dehydrated using 100% alcohol, transferred to xylene, and mounted in DPX for further imaging.

Initially, rehydrated tissue sections were used for immunohistochemical analysis. Specific antigen retrievals were performed for ColII, ColX, ColI, NFκB, and pSMAD1/5/9. Acidic 0.05% pepsin was employed for 30 min at 37°C to detect collagen. For pSMAD1/5/9 and NFκB, citrate buffer retrieval (pH 6.0) was used. Then, the tissue sections were rinsed with PBT three times, each for 10 min. To avoid nonspecific binding, tissue sections were incubated in 5% goat serum for 1 h. Afterward, they were incubated with primary antibodies against collagen type X (DSHB X-AC9s, 1:20), collagen type II (DSHB CIICI, 1:20), ColI polyclonal antibody (PA1-85319, Invitrogen), NFκB (CST Cat. no. 8242S), and pSMAD1/5/9 (CST, Cat. no.13820S, 1:100) overnight at 4°C. Then, the tissue sections were rinsed with PBST and incubated with a fluorescently labeled secondary antibody (dilution 1:250) for 3–4 h at room temperature. Tissue sections were further incubated with DAPI (1:1000) for 15 min after antibody incubation, then mounted in antifade solution and imaged using a Leica DM5000B compound microscope.

5.5.10 | Blind Data Scoring

Tissue sections stained with Safranin O were graded according to the standards set by the Osteoarthritis Research Society International (OARSI) by three independent experts who were not principally involved in the in vivo experiment. All sections were scored blindly on a 0–6 scale. OA alterations are mild in those with scores 0–2, while significant cartilage erosion is indicated by scores 3–6.

5.6 | Statistical Analysis

GraphPad Prism 7.1 software was used to ascertain the statistical significance of the OARSI scoring histopathological data. A nonparametric ANOVA with post hoc analysis (Tukey's multiple-comparison test) was performed to simultaneously compare the four experimental groups. The error bar in the graphs is the Standard Deviation (SD) from the mean. For in vitro characterization, multiple comparisons were analyzed using a one-way ANOVA with post hoc analysis (Tukey's multiple comparison test), whereas a nonparametric *t*-test was used to compare two experimental groups.

Author Contributions

Sayeda Fauzia Iqbal: conceptualization, methodology, investigation, visualization, validation, formal analysis, data curation, project administration, and writing – original draft. **Nilotpal Majumder**: conceptualization, methodology, investigation, visualization, validation, formal analysis, data curation, project administration, and writing – original draft. **Bhupendra Kumar**: investigation and methodology. **Chandrashish Roy**: methodology and formal analysis. **Saahiba Thaleshwari**: formal analysis. **Sourabh Ghosh**: conceptualization, supervision, resources, funding acquisition, project administration, writing – review, and editing. **Amitabha Bandyopadhyay**: conceptualization, supervision, resources, funding acquisition, project administration, writing – review, and editing.

Acknowledgements

We sincerely thank the Department of Biotechnology (DBT), Government of India (BT/IN/Swiss/54/SG/2018-19) for funding this research work. We also thank 5/3/8/20/2019-ITR (ICMR) and BT/PR/45389/CMD/150/11/2022 (DBT) for providing funding and support. All the micro-CT data were generated using a central facility established through a FIST grant from the Department of Science and Technology (SR/FST/LSII-033/2014). We sincerely thank Mrs. Shraddha Singh for providing technical help with micro-CT imaging. The authors are immensely grateful to the Central Experimental Animal Facility (CEAF), IIT Kanpur, and Ms. Sweta Kushwaha for technical assistance with confocal imaging.

Conflicts of Interest

The authors declare no conflicts of interest.

Data Availability Statement

The data that support the findings of this study are available from the corresponding author upon reasonable request.

References

1. J. D. Steinmetz, G. T. Culbreth, L. M. Haile, et al., "Global, Regional, and National Burden of Osteoarthritis, 1990–2020 and Projections to 2050: A Systematic Analysis for the Global Burden of Disease Study 2021," *The Lancet Rheumatology* 5 (2023): e508–e522, https://doi.org/10.1016/S2665-9913(23)00163-7.

2. Q. Yao, X. Wu, C. Tao, et al., "Osteoarthritis: Pathogenic Signaling Pathways and Therapeutic Targets," *Signal Transduction and Targeted Therapy* 8 (2023): 56, https://doi.org/10.1038/s41392-023-01330-w.

3. M. Binvignat, J. Sellam, F. Berenbaum, and D. T. Felson, "The Role of Obesity and Adipose Tissue Dysfunction in Osteoarthritis Pain," *Nature Reviews Rheumatology* 20 (2024): 565–584, https://doi.org/10.1038/s41584-024-01143-3.

4. B. A. Kornah, H. M. Safwat, S. K. Abdel-hameed, et al., "Managing of Post-Traumatic Knee Arthritis by Total Knee Arthroplasty: Case Series of 15 Patients and Literature Review," *Journal of Orthopaedic Surgery and Research* 14 (2019): 168, https://doi.org/10.1186/s13018-019-1180-3.

5. T. Blikman, W. Rienstra, T. M. van Raaij, et al., "Duloxetine in OsteoArthritis (DOA) Study: Effects of Duloxetine on Pain and Function in End-Stage Hip and Knee OA—A Pragmatic Enriched Randomized Controlled Trial," *BMC Musculoskeletal Disorders* 23 (2022): 115, https://doi.org/10.1186/s12891-022-05034-0.

6. L. A. Vonk, "Key Insights and Implications of Cartilage Degradation in Osteoarthritis," *Connective Tissue Research* 66 (2025): 393–398, https://doi.org/10.1080/03008207.2025.2536153.

7. J. Chakraborty, N. Majumder, A. Sharma, S. Prasad, and S. Ghosh, "3D Bioprinted Silk-Reinforced Alginate-Gellan Gum Constructs for Cartilage Regeneration," *Bioprinting* 28 (2022): e00232, https://doi.org/10.1016/j.bprint.2022.e00232.

8. A. Bandyopadhyay, B. B. Mandal, and N. Bhardwaj, "3D Bioprinting of Photo-Crosslinkable Silk Methacrylate (SilMA)-Polyethylene Glycol Diacrylate (PEGDA) Bioink for Cartilage Tissue Engineering," *Journal of Biomedical Materials Research Part A* 110 (2022): 884–898, https://doi.org/10.1002/jbm.a.37336.

9. N. Majumder, S. Seit, N. S. Bhabesh, and S. Ghosh, "An Advanced Bioconjugation Strategy for Covalent Tethering of TGFβ3 with Silk Fibroin Matrices and Its Implications in the Chondrogenesis Profile of Human BMSCs and Human Chondrocytes: A Paradigm Shift in Cartilage Tissue Engineering," *Advanced Healthcare Materials* 13 (2024): 2303513, https://doi.org/10.1002/adhm.202303513.

10. J. Lee, C. Y. Lee, J.-H. Park, et al., "Differentiation of Adipose-Derived Stem Cells into Functional Chondrocytes by a Small Molecule That Induces Sox9," *Experimental & Molecular Medicine* 52 (2020): 672–681, https://doi.org/10.1038/s12276-020-0424-y.

11. I. Bdikin and P. A. A. P. Marques, "Electrospinning of Bioactive Polycaprolactone-Gelatin Nanofibres with Increased Pore Size for Cartilage Tissue Engineering Applications," *Journal of Biomaterials Applications* 35 (2020): 471–484.

12. N. Majumder, S. Roy, A. Sharma, et al., "Assessing the Advantages of 3D Bioprinting and 3D Spheroids in Deciphering the Osteoarthritis Healing Mechanism Using Human Chondrocytes and Polarized Macrophages," *Biomedical Materials* 19 (2024): 025005, https://doi.org/10.1088/1748-605X/ad1d18.

13. S. Shimomura, H. Inoue, Y. Arai, et al., "Hypoxia Promotes Differentiation of Pure Cartilage from Human Induced Pluripotent Stem Cells," *Molecular Medicine Reports* 26 (2022): 229, https://doi.org/10.3892/mmr.2022.12745.

14. M. Bhattacharjee, J. Coburn, M. Centola, et al., "Tissue Engineering Strategies to Study Cartilage Development, Degeneration and Regeneration," *Advanced Drug Delivery Reviews* 84 (2015): 107–122, https://doi.org/10.1016/j.addr.2014.08.010.

15. L. de Roy, G. Q. Teixeira, J. Schwer, et al., "Structure-Function of Cartilage in Osteoarthritis: an Ex-Vivo Correlation Analysis between its Structural, Viscoelastic and Frictional Properties," *Acta Biomaterialia* 190 (2024): 293–302, https://doi.org/10.1016/j.actbio.2024.10.027.

16. P. Lepetsos and A. G. Papavassiliou, "ROS/Oxidative Stress Signaling in Osteoarthritis," *Biochimica et Biophysica Acta—Molecular Basis of Disease* 1862 (2016): 576–591.

17. H. Stanton, F. M. Rogerson, C. J. East, et al., "ADAMTS5 is the Major Aggrecanase in Mouse Cartilage in Vivo and in Vitro," *Nature* 434 (2005): 648–652, https://doi.org/10.1038/nature03417.

18. J. Zhou, Q. Chen, B. Lanske, et al., "Disrupting the Indian Hedgehog Signaling Pathway in Vivo Attenuates Surgically Induced Osteoarthritis Progression in Col2a1-CreERT2; Ihhfl/fl Mice," *Arthritis Research & Therapy* 16 (2014): R11, https://doi.org/10.1186/ar4437.

19. C. Zhang, R. Zhao, Z. Dong, et al., "IHH–GLI-1–HIF-2α Signalling Influences Hypertrophic Chondrocytes to Exacerbate Osteoarthritis Progression," *Journal of Orthopaedic Translation* 49 (2024): 207–217, https://doi.org/10.1016/j.jot.2024.09.008.

20. A. P. Jaswal, B. Kumar, A. J. Roelofs, et al., "BMP Signaling: a Significant Player and Therapeutic Target for Osteoarthritis," *Osteoarthritis and Cartilage* 31 (2023): 1454–1468, https://doi.org/10.1016/j.joca.2023.05.016.

21. N. Majumder and S. Ghosh, "Unfolding the Mystery behind the Onset of Chondrocyte Hypertrophy during Chondrogenesis: toward Designing Advanced Permanent Cartilage-Mimetic Biomaterials," *Advanced Functional Materials* 33 (2023): 2300651, https://doi.org/10.1002/adfm.202300651.

22. J. H. Ryu, Y. Shin, Y. H. Huh, S. Yang, C.-H. Chun, and J.-S. Chun, "Hypoxia-Inducible Factor-2α Regulates Fas-Mediated Chondrocyte Apoptosis during Osteoarthritic Cartilage Destruction," *Cell Death & Differentiation* 19 (2012): 440–450, https://doi.org/10.1038/cdd.2011.111.

23. Y. Wu, A. Li, N. Sun, et al., "Unveiling the Mechanisms of Mechanical Loading-Induced Knee Osteoarthritis through Transcriptomics," *International Immunopharmacology* 157 (2025): 114785, https://doi.org/10.1016/j.intimp.2025.114785.

24. T. Nakase, T. Miyaji, T. Tomita, et al., "Localization of Bone Morphogenetic Protein-2 in Human Osteoarthritic Cartilage and Osteophyte," *Osteoarthritis and Cartilage* 11 (2003): 278–284, https://doi.org/10.1016/S1063-4584(03)00004-9.

25. P. Occhetta, S. Pigeot, M. Rasponi, et al., "Developmentally Inspired Programming of Adult Human Mesenchymal Stromal Cells toward Stable Chondrogenesis," *Proceedings of the National Academy of Sciences* 115 (2018): 4625–4630, https://doi.org/10.1073/pnas.1720658115.

26. S. Chawla, S. Midha, A. Sharma, and S. Ghosh, "Silk-Based Bioinks for 3D Bioprinting," *Advanced Healthcare Materials* 7 (2018): 1701204, https://doi.org/10.1002/adhm.201701204.

27. J. Fritz, A.-C. Moser, A. Otahal, et al., "Silk Fibroin-Based Hydrogels Supplemented with Decellularized Extracellular Matrix and Gelatin Facilitate 3D Bioprinting for Meniscus Tissue Engineering," *Macromolecular Bioscience* 25 (2025): 2400515, https://doi.org/10.1002/mabi.202400515.

28. S. Chawla, A. Sharma, A. Bandyopadhyay, and S. Ghosh, "Developmental Biology-Inspired Strategies to Engineer 3D Bioprinted Bone Construct," *ACS Biomaterials Science & Engineering* 4 (2018): 3545–3560, https://doi.org/10.1021/acsbiomaterials.8b00757.

29. C. Phamornnak, B. Han, B. F. Spencer, et al., "Instructive Electroactive Electrospun Silk Fibroin-Based Biomaterials for Peripheral Nerve Tissue Engineering," *Biomaterials Advances* 141 (2022): 213094, https://doi.org/10.1016/j.bioadv.2022.213094.

30. P. Admane, A. C. Gupta, P. Jois, et al., "Direct 3D Bioprinted Full-Thickness Skin Constructs Recapitulate Regulatory Signaling Pathways and Physiology of Human Skin," *Bioprinting* 15 (2019): e00051, https://doi.org/10.1016/j.bprint.2019.e00051.

31. S. Chameettachal, S. Midha, and S. Ghosh, "Regulation of Chondrogenesis and Hypertrophy in Silk Fibroin-Gelatin-Based 3D Bioprinted Constructs," *ACS Biomaterials Science & Engineering* 2 (2016): 1450–1463, https://doi.org/10.1021/acsbiomaterials.6b00152.

32. S. Chawla, A. Kumar, P. Admane, A. Bandyopadhyay, and S. Ghosh, "Elucidating Role of Silk-Gelatin Bioink to Recapitulate Articular Cartilage Differentiation in 3D Bioprinted Constructs," *Bioprinting* 7 (2017): 1–13, https://doi.org/10.1016/j.bprint.2017.05.001.

33. S. Chawla, G. Desando, E. Gabusi, et al., "The Effect of Silk–Gelatin Bioink and TGF-β3 on Mesenchymal Stromal Cells in 3D Bioprinted Chondrogenic Constructs: a Proteomic Study," *Journal of Materials Research* 36 (2021): 4051–4067.

34. S. Chawla, A. Mainardi, N. Majumder, et al., "Chondrocyte Hypertrophy in Osteoarthritis: Mechanistic Studies and Models for the Identification of New Therapeutic Strategies," *Cells* 11 (2022): 4034, https://doi.org/10.3390/cells11244034.

35. N. Majumder, C. Roy, L. Doenges, I. Martin, A. Barbero, and S. Ghosh, "Covalent Conjugation of Small Molecule Inhibitors and Growth Factors to a Silk Fibroin-Derived Bioink to Develop Phenotypically Stable 3D Bioprinted Cartilage," *ACS Applied Materials & Interfaces* 16 (2024): 9925–9943, https://doi.org/10.1021/acsami.3c18903.

36. A. Dufour, J. E. Lafont, M. Buffier, et al., "Repair of Full-Thickness Articular Cartilage Defects Using IEIK13 Self-Assembling Peptide Hydrogel in a Non-Human Primate Model," *Scientific Reports* 11 (2021): 4560, https://doi.org/10.1038/s41598-021-83208-x.

37. K. Sun, R. Li, and M. Fan, "Repair of Full-Thickness Articular Cartilage Defects with a 3DP-Anchored Three-Phase Complex," *Heliyon* 9 (2023): e21123, https://doi.org/10.1016/j.heliyon.2023.e21123.

38. B. Haberal, O. Sahin, A. Terzi, E. K. Simsek, A. Mahmuti, and I. C. Tuncay, "Treatment of Full-Thickness Cartilage Defects with Pedunculated and Free Synovial Grafts: a Comparative Study in an Animal Model," *Indian Journal of Orthopaedics* 54 (2020): 720–725, https://doi.org/10.1007/s43465-020-00067-w.

39. L. Zhou, J. Xu, A. Schwab, et al., "Engineered Biochemical Cues of Regenerative Biomaterials to Enhance Endogenous Stem/Progenitor Cells (ESPCs)-Mediated Articular Cartilage Repair," *Bioactive Materials* 26 (2023): 490–512, https://doi.org/10.1016/j.bioactmat.2023.03.008.

40. C. Vinatier and J. Guicheux, "Cartilage Tissue Engineering: from Biomaterials and Stem Cells to Osteoarthritis Treatments," *Annals of Physical and Rehabilitation Medicine* 59 (2016): 139–144, https://doi.org/10.1016/j.rehab.2016.03.002.

41. P. S. Yadav, P. Prashar, and A. Bandyopadhyay, "BRITER: a BMP Responsive Osteoblast Reporter Cell Line," *PLoS ONE* 7 (2012): 37134, https://doi.org/10.1371/journal.pone.0037134.

42. S. Rigoglou and A. G. Papavassiliou, "The NF-κB Signalling Pathway in Osteoarthritis," *The International Journal of Biochemistry & Cell Biology* 45 (2013): 2580–2584, https://doi.org/10.1016/j.biocel.2013.08.018.

43. N. Sahai, M. Gogoi, and R. P. Tewari, "3D Printed Chitosan Composite Scaffold for Chondrocytes Differentiation," *Current Medical Imaging Formerly Current Medical Imaging Reviews* 17 (2020): 832–842, https://doi.org/10.2174/1573405616666201217112939.

44. X. Hu, M. Jin, K. Sun, et al., "Type II Collagen Scaffolds Repair Critical-Sized Osteochondral Defects under Induced Conditions of Osteoarthritis in Rat Knee Joints via Inhibiting TGF-β-Smad1/5/8 Signaling Pathway," *Bioactive Materials* 35 (2024): 416–428.

45. Q. Li, S. Xu, Q. Feng, et al., "3D Printed Silk-Gelatin Hydrogel Scaffold with Different Porous Structure and Cell Seeding Strategy for Cartilage Regeneration," *Bioactive Materials* 6 (2021): 3396–3410.

46. S. Das, F. Pati, S. Chameettachal, et al., "Enhanced Redifferentiation of Chondrocytes on Microperiodic Silk/Gelatin Scaffolds: Toward Tailor-Made Tissue Engineering," *Biomacromolecules* 14 (2013): 311–321, https://doi.org/10.1021/bm301193t.

47. H. H. Yoon, S. H. Bhang, J.-Y. Shin, J. Shin, and B.-S. Kim, "Enhanced Cartilage Formation via Three-Dimensional Cell Engineering of Human Adipose-Derived Stem Cells," *Tissue Engineering Part A* 18 (2012): 1949–1956, https://doi.org/10.1089/ten.tea.2011.0647.

48. P. S. Yadav, M. P. Khan, P. Prashar, et al., "Characterization of BMP Signaling Dependent Osteogenesis Using a BMP Depletable Avianized Bone Marrow Stromal Cell Line (TVA-BMSC)," *Bone* 91 (2016): 39–52, https://doi.org/10.1016/j.bone.2016.07.010.

49. A. K. Gill, P. J. McCormick, D. Sochart, and G. Nalesso, "Wnt Signalling in the Articular Cartilage: A Matter of Balance," *International Journal of Experimental Pathology* 104 (2023): 56–63, https://doi.org/10.1111/iep.12472.

50. T. Biswas, A. P. Jaswal, U. S. Yadav, and A. Bandyopadhyay, "Simultaneous Differentiation of Articular and Transient Cartilage: WNT-BMP Interplay and Its Therapeutic Implication," *The International Journal of Developmental Biology* 64 (2020): 203–211, https://doi.org/10.1387/ijdb.190149ab.

51. J. Chakraborty, J. Fernández-Pérez, K. A. van Kampen, et al., "Development of a Biomimetic Arch-Like 3D Bioprinted Construct for Cartilage Regeneration Using Gelatin Methacryloyl and Silk Fibroin-Gelatin Bioinks," *Biofabrication* 15 (2023): 035009, https://doi.org/10.1088/1758-5090/acc68f.

52. N. Majumder, A. Mishra, and S. Ghosh, "Effect of Varying Cell Densities on the Rheological Properties of the Bioink," *Bioprinting* 28 (2022): e00241, https://doi.org/10.1016/j.bprint.2022.e00241.

53. E. C. Beck, M. Barragan, M. H. Tadros, S. H. Gehrke, and M. S. Detamore, "Approaching the Compressive Modulus of Articular Cartilage with a Decellularized Cartilage-Based Hydrogel," *Acta Biomaterialia* 38 (2016): 94–105, https://doi.org/10.1016/j.actbio.2016.04.019.

54. X. Hu, K. Shmelev, L. Sun, et al., "Regulation of Silk Material Structure by Temperature-Controlled Water Vapor Annealing," *Biomacromolecules* 12 (2011): 1686–1696, https://doi.org/10.1021/bm200062a.

55. K. Yazawa, K. Ishida, H. Masunaga, T. Hikima, and K. Numata, "Influence of Water Content on the β-Sheet Formation, Thermal Stability, Water Removal, and Mechanical Properties of Silk Materials," *Biomacromolecules* 17 (2016): 1057–1066, https://doi.org/10.1021/acs.biomac.5b01685.

56. Y. Kambe, Y. Mizoguchi, K. Kuwahara, T. Nakaoki, Y. Hirano, and T. Yamaoka, "Beta-Sheet Content Significantly Correlates with the Biodegradation Time of Silk Fibroin Hydrogels Showing a Wide Range of Compressive Modulus," *Polymer Degradation and Stability* 179 (2020): 109240, https://doi.org/10.1016/j.polymdegradstab.2020.109240.

57. J. Chakraborty, J. Fernández-Pérez, M. Takhsha Ghahfarokhi, et al., "Development of 4D-Bioprinted Shape-Morphing Magnetic Constructs for Cartilage Regeneration Using a Silk Fibroin-Gelatin Bioink," *Cell*

Reports Physical Science 5 (2024): 101819, https://doi.org/10.1016/j.xcrp.2024.101819.

58. T. Chen, M. J. Hilton, E. B. Brown, M. J. Zuscik, and H. A. Awad, "Engineering Superficial Zone Features in Tissue Engineered Cartilage," *Biotechnology and Bioengineering* 110 (2013): 1476–1486, https://doi.org/10.1002/bit.24799.

59. B. S. Yoon, D. A. Ovchinnikov, I. Yoshii, Y. Mishina, R. R. Behringer, and K. M. Lyons, "Bmpr1a and Bmpr1b Have Overlapping Functions and Are Essential for Chondrogenesis in Vivo," *Proceedings of the National Academy of Sciences* 102 (2005): 5062–5067, https://doi.org/10.1073/pnas.0500031102.

60. Y. Park, M. Sugimoto, A. Watrin, M. Chiquet, and E. B. Hunziker, "BMP-2 Induces the Expression of Chondrocyte-Specific Genes in Bovine Synovium-Derived Progenitor Cells Cultured in Three-Dimensional Alginate Hydrogel," *Osteoarthritis and Cartilage* 13 (2005): 527–536, https://doi.org/10.1016/j.joca.2005.02.006.

61. M. M. J. Caron, M. Eveque, B. Cillero-Pastor, et al., "Sox9 Determines Translational Capacity during Early Chondrogenic Differentiation of ATDC5 Cells by Regulating Expression of Ribosome Biogenesis Factors and Ribosomal Proteins," *Frontiers in Cell and Developmental Biology* 9 (2021): 686096, https://doi.org/10.3389/fcell.2021.686096.

62. H. Ma, B. Xie, H. Chen, et al., "High-Strength and High-Elasticity Silk Fibroin-Composite Gelatin Biomaterial Hydrogels for Rabbit Knee Cartilage Regeneration," *Frontiers in Materials* 11 (2024): 1390372, https://doi.org/10.3389/fmats.2024.1390372.

63. S. Yu, X. Shu, L. Chen, et al., "Construction of Ultrasonically Treated Collagen/Silk Fibroin Composite Scaffolds to Induce Cartilage Regeneration," *Scientific Reports* 13 (2023): 20168, https://doi.org/10.1038/s41598-023-43397-z.

64. Y. Shen, Y. Xu, B. Yi, et al., "Engineering a Highly Biomimetic Chitosan-Based Cartilage Scaffold by Using Short Fibers and a Cartilage-Decellularized Matrix," *Biomacromolecules* 22 (2021): 2284–2297, https://doi.org/10.1021/acs.biomac.1c00366.

65. Z. Wu, S. H. Korntner, A. M. Mullen, and D. I. Zeugolis, "Collagen Type II: from Biosynthesis to Advanced Biomaterials for Cartilage Engineering," *Biomaterials and Biosystems* 4 (2021): 100030, https://doi.org/10.1016/j.bbiosy.2021.100030.

66. R. A. G. Franco, E. McKenna, P. G. Robey, et al., "Inhibition of BMP Signaling with LDN 193189 Can Influence Bone Marrow Stromal Cell Fate but Does Not Prevent Hypertrophy during Chondrogenesis," *Stem Cell Reports* 17 (2022): 616–632, https://doi.org/10.1016/j.stemcr.2022.01.016.

67. J. H. Boergermann, J. Kopf, P. B. Yu, and P. Knaus, "Dorsomorphin and LDN-193189 Inhibit BMP-Mediated Smad, p38 and Akt Signalling in C2C12 Cells," *The International Journal of Biochemistry & Cell Biology* 42 (2010): 1802–1807, https://doi.org/10.1016/j.biocel.2010.07.018.

68. J. Gu, Y. Lu, F. Li, et al., "Identification and Characterization of the Novel Col10a1 Regulatory Mechanism during Chondrocyte Hypertrophic Differentiation," *Cell Death & Disease* 5 (2014): e1469–e1469, https://doi.org/10.1038/cddis.2014.444.

69. Y. He, A. S. Siebuhr, N. U. Brandt-Hansen, et al., "Type X Collagen Levels Are Elevated in Serum from Human Osteoarthritis Patients and Associated with Biomarkers of Cartilage Degradation and Inflammation," *BMC Musculoskeletal Disorders* 15 (2014): 309, https://doi.org/10.1186/1471-2474-15-309.

70. M. Tschaikowsky, S. Brander, V. Barth, et al., "The Articular Cartilage Surface Is Impaired by a Loss of Thick Collagen Fibers and Formation of Type I Collagen in Early Osteoarthritis," *Acta Biomaterialia* 146 (2022): 274–283, https://doi.org/10.1016/j.actbio.2022.04.036.

71. S. Semenistaja, L. Sokolovska, S. Svirskis, P. Studers, V. Groma, and S. Skuja, "Distinct Late-Stage Osteoarthritis Profiles Identified through NF-κB, TNF-α, and TGF-β–driven Synovial Inflammation and Pain," *Scientific Reports* 15 (2025): 30288, https://doi.org/10.1038/s41598-025-16078-2.

72. S. J. Song and C. H. Park, "urrent Concepts and Limitations of Systematic Reviews," *Annals of Translational Medicine* 7 (2019): S108, https://doi.org/10.21037/atm.2019.05.11.

73. N. Schizas, O. Savvidou, I. Triantafyllopoulos, S. Papadakis, I. Dontas, and P. Papagelopoulos, "Adjuvant Therapies for the Enhancement of Microfracture Technique in Cartilage Repair," *Orthopedic Reviews* 11 (2019): 7950, https://doi.org/10.4081/or.2019.7950.

74. J. M. Lee and G. I. Im, "SOX Trio-Co-Transduced Adipose Stem Cells in Fibrin Gel to Enhance Cartilage Repair and Delay the Progression of Osteoarthritis in the Rat," *Biomaterials* 33 (2012): 2016–2024, https://doi.org/10.1016/j.biomaterials.2011.11.050.

75. N. Yusop, P. Battersby, A. Alraies, A. J. Sloan, R. Moseley, and R. J. Waddington, "Isolation and Characterisation of Mesenchymal Stem Cells from Rat Bone Marrow and the Endosteal Niche: a Comparative Study," *Stem Cells International* 2018 (2018): 6869128.

76. U. Kumarasinghe, N. Majumder, J. M. Sutaria, et al., "Temporary Silk Nanocoatings Preserve Immune Cell Functions and Protection against Biochemical and Mechanical Stressors," *Biomaterials* 325 (2026): 123605, https://doi.org/10.1016/j.biomaterials.2025.123605.

77. S. Roy, A. Sharma, and S. Ghosh, "Macrophage Polarization Profiling on Native and Regenerated Silk Biomaterials," *ACS Biomaterials Science & Engineering* 8 (2022): 659–671, https://doi.org/10.1021/acsbiomaterials.1c01432.

78. W. N. Arifin and W. M. Zahiruddin, "Sample Size Calculation in Animal Studies Using Resource Equation Approach," *Malaysian Journal of Medical Sciences* 24 (2017): 101.

Supporting Information

Additional supporting information can be found online in the Supporting Information section.

Supporting File: adhm71252-sup-0001-SuppMat.docx.